ENGINEERING RESEARCH INSTITUTE
UNIVERSITY OF MICHIGAN
ANN ARBOR

FLOW AND TORQUE CHARACTERISTICS OF BUTTERFLY VALVES AT SUBCRITICAL AND SUPERCRITICAL PRESSURE RATIOS

BY

HENRY H. HICKS, JR.

L. C. GARBY

ALBERT STOHRER

FRANK A. REID

Project M932

SVERDRUP AND PARCEL, INC.
ST. LOUIS, MISSOURI

October, 1952

TABLE OF CONTENTS

LIST OF FIGURES

List of Figures (cont.)

LIST OF SYMBOLS

A surface area or duct area

b a constant

C specific heat

C_f valve flow coefficient

C_t dimensionless torque coefficient

h heat-transfer coefficient

K orifice coefficient

k heat capacity ratio

L heat of fusion

M mass in lbs or Mach number

m mass in lbs

n (k-1)/k

n_1, n_2, n_3 constants

p pressure on an absolute scale

P_R pressure ratio

P_{v1}, P_{v2}, P_{v3} pressure referred to valve plate - taps 1, 2, and 3

Q mass flow

q heat flux

r pressure ratio P_2/P_o

T temperature, °R or °F

t time

V linear velocity

w mass flow rate

Y expansion factor for an orifice

Subscripts

1 Static stream quantities upstream of valve

2 Static stream quantities downstream of valve

0 Total stream quantities upstream of valve

SUMMARY

Torque and flow characteristics of circular and segmental butterfly valves have been determined as a function of valve angle and static pressure ratio across the value. Pressures on the faces and on the edge of the valve plate have also been related to valve angle and pressure ratio. In addition, a study has been made of the blowdown temperature relationships in the air supply tank.

The flow coefficient C_f was defined in an earlier report* for the case of supercritical flows as the ratio of the actual mass flow through the valve to the flow through an opening equal to the projected opening of the valve, assuming a straight sonic line at the opening. For the case of subcritical pressure ratios presented in this report, the same form is used for the flow coefficient, except that a sonic line can no longer be assumed at the opening. For the subcritical case, the conditions at the opening are computed assuming isentropic compressible flow into the opening.

The flow coefficient is determined by the valve angle and the pressure ratio across the valve, but the primary effect is due to valve angle. The average valve of C_f for the circular valve is about 0.70 for a pressure ratio of 1.0 and approaches a valve of 0.90 for pressure ratios of 2.0 and greater (see Fig. 23). The values of C_f for the segmental valves are changed considerably by valve angle, so that no generalization appears possible, (see Fig. 40).

Valve torque is a function of valve angle, pressure ratio across the valve, and absolute upstream pressure. The torque reaches a maximum for a valve angle of about 70° measured from the closed position. The torque apparently becomes a linear function of absolute upstream pressure for pressure ratios greater than about 2.0, (see Fig. 32).

Valve plate pressure on the upstream face of the plate is closely related to the upstream total pressure. The pressure on the edge of the valve plate is closely related to the static pressure in the valve opening. The pressure on the downstream face of the valve plate lies between the downstream static pressure and the static pressure in the valve opening. A change in valve angle has little effect on the pressure on the upstream face of the valve plate, but has a large influence on the pressure on the downstream face and at the edge of the valve plate, (see Figs. 14-19 and 34-39).

The air-tank blowdown curves show that the relative approach to an isentropic expansion is governed by the rate of blowdown. The approach does not appear to be linear with respect to blowdown rate, however. In other words, a close approach to isentropic expansion of the air in the tank would require a very rapid discharge rate.

---

* Flow Characteristics of A Butterfly Valve at Supercritical Pressure Ratios, L. C. Garby, H. H. Hicks, J. S. Murphy, 15 June 1951, University of Michigan, Engineering Research Institute.

There is a temperature lag between a thermocouple element and the air surrounding it when the air temperature is changing. A method for evaluating this lag for conditions inside the tank is discussed.

FLOW AND TORQUE CHARACTERISTICS OF BUTTERFLY VALVES AT SUBCRITICAL AND SUPERCRITICAL PRESSURE RATIOS

INTRODUCTION

This report presents the results of a test program* on butterfly valves that has been carried on for a period of about a year at the University of Michigan Aircraft Propulsion Laboratory.** The program was initiated for the purpose of investigating the valve flow characteristics for supercritical pressure ratios. Adequate data were not previously available for these conditions. As the work progressed, it became apparent that the valve torque would also have to be investigated, since for practical valve design this information may be as important as the flow data. Later, the flow investigation was extended into the subcritical pressure ratios.

Independent of the valve work, the contractors* requested that an investigation be made of pressure and temperature conditions inside the large air storage tank (Figs. 2, 7) during blowdown. This study has been conducted simultaneously with the valve work.

The authors wish to acknowledge the valuable assistance of Professor Wilbur C. Nelson[1] and Dr. R. B. Morrison[2], who gave continued technical assistance during the course of the work.

---

*This program has been carried on as a subcontract with Sverdrup and Parcel, Inc., Consulting Engineers, St. Louis, Mo., Contract AF 33(038)9928.

**Formerly, University of Michigan Combustion Research Laboratory

1 University of Michigan, Department of Aeronautical Engineering

2 University of Michigan, Aircraft Propulsion Laboratory

I. DESCRIPTION OF EQUIPMENT AND DISCUSSION OF TESTING TECHNIQUE

Air Circuit

The air supply for the valve testing comes from a blowdown system, (Fig. 1). Two large steel tanks (Fig. 2) having total capacities of 170 cu ft and working pressures of 3500 psi are charged by two Ingersoll-Rand four-stage air compressors. The combined free-air capacity of the compressors is 140 cu ft/min. This gives a tank changing time of about 4 hours, during which approximately 2000 lbs mass of air is charged. The tanks are manifolded together and the air is carried to the test site through about 100 feet of 2-1/2-inch (schedule-160) steel pipe. At the test site the air is throttled to a constant pressure of 300-500 psig by means of a 2-1/2-inch Forster regulating valve. The regulated air is then fed into the test setup through a 1-inch hand-operated gate valve. For convenience of adjustment, this valve is bypassed by a 1/4-inch hand-operated globe valve. Following the hand-control valve there is a length of 6-inch schedule-80 steel pipe, in which the flow orifice is located. Means are provided for measuring upstream static air pressure and the differential pressure at the orifice. The temperature of the air is measured ahead of the orifice by means of a submerged thermocouple. Three sizes of square-edged orifices were used to accommodate the flow range, these being circular and having diameters of 1, 2, and 4 inches.*

Means are provided for measuring upstream and downstream static pressure at the butterfly valve, and for certain tests upstream total pressure was measured. For the early tests which were run on the circular valve, total head rakes were placed in the pipe upstream and down stream of the valve. The data taken from these rakes did not directly correlate with valve characteristics, so the rakes were abandoned during later testing. At the exit of the system, a hand-controlled gate valve in the 6-inch line controls the pressure downstream of the valve (Figs. 1, 3, and 4).

Valve Plate Pressures

The valve plate pressures are picked up by surface taps and are transmitted through small tubes which are brought out through the valve shaft. These pressures are measured with manometers or with Bourdon tube gauges, depending on the magnitude of the pressures (Figs. 12 and 28). The Bourdon tube gauges used have a maximum error of about 5 per cent.

* See Appendix II for details of orifice calibration.

AIR CIRCUIT USED IN VALVE TESTS

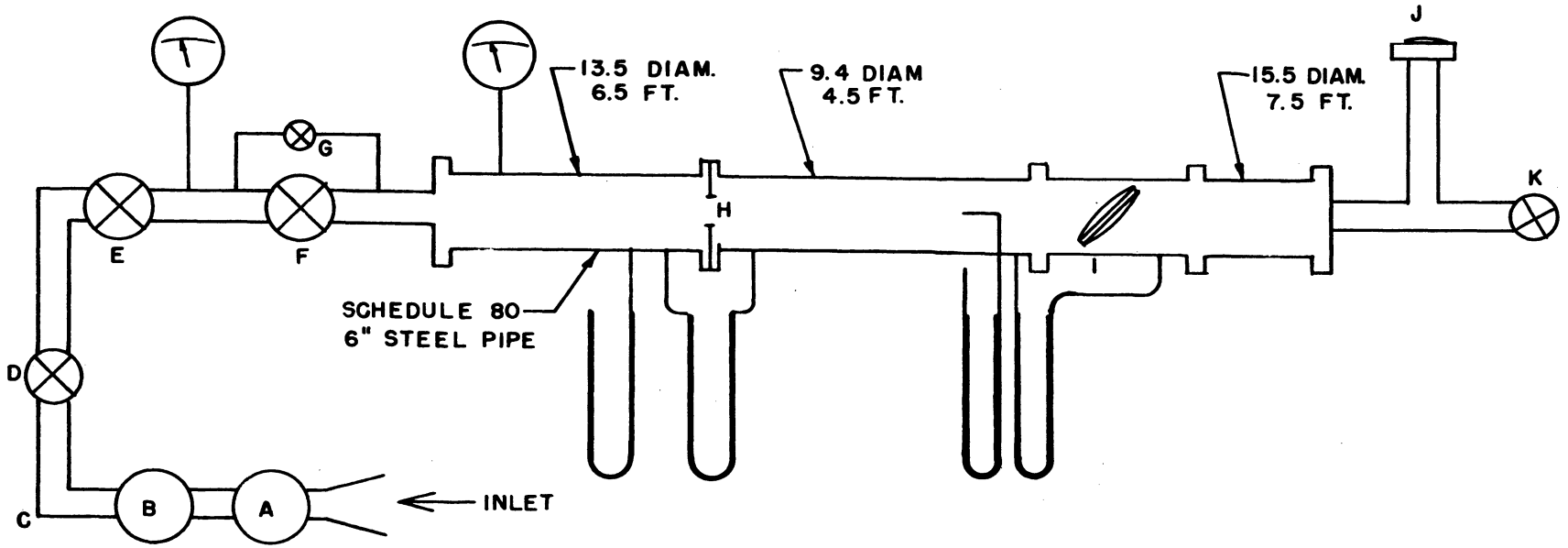

A- AIR COMPRESSORS - 140 CFM FREE AIR TO 3500 PSI
B- ACCUMULATORS
C- 100FT, $2\frac{1}{2}$"- SCHEDULE 160 STEEL PIPE
D- MAIN ON-OFF VALVE
E- PRESSURE REGULATOR
F- HAND CONTROL VALVE
G- BY PASS VALVE
H- ORFICE PLATE, RADIUS TAPS
I - BUTTER VALVE (CIRCULAR OR SEGMENTED)
J- SAFETY DIAPHRAGM
K- DOWN STREAM PRESSURE CONTROL VALVE

AWS

FIG. 1.

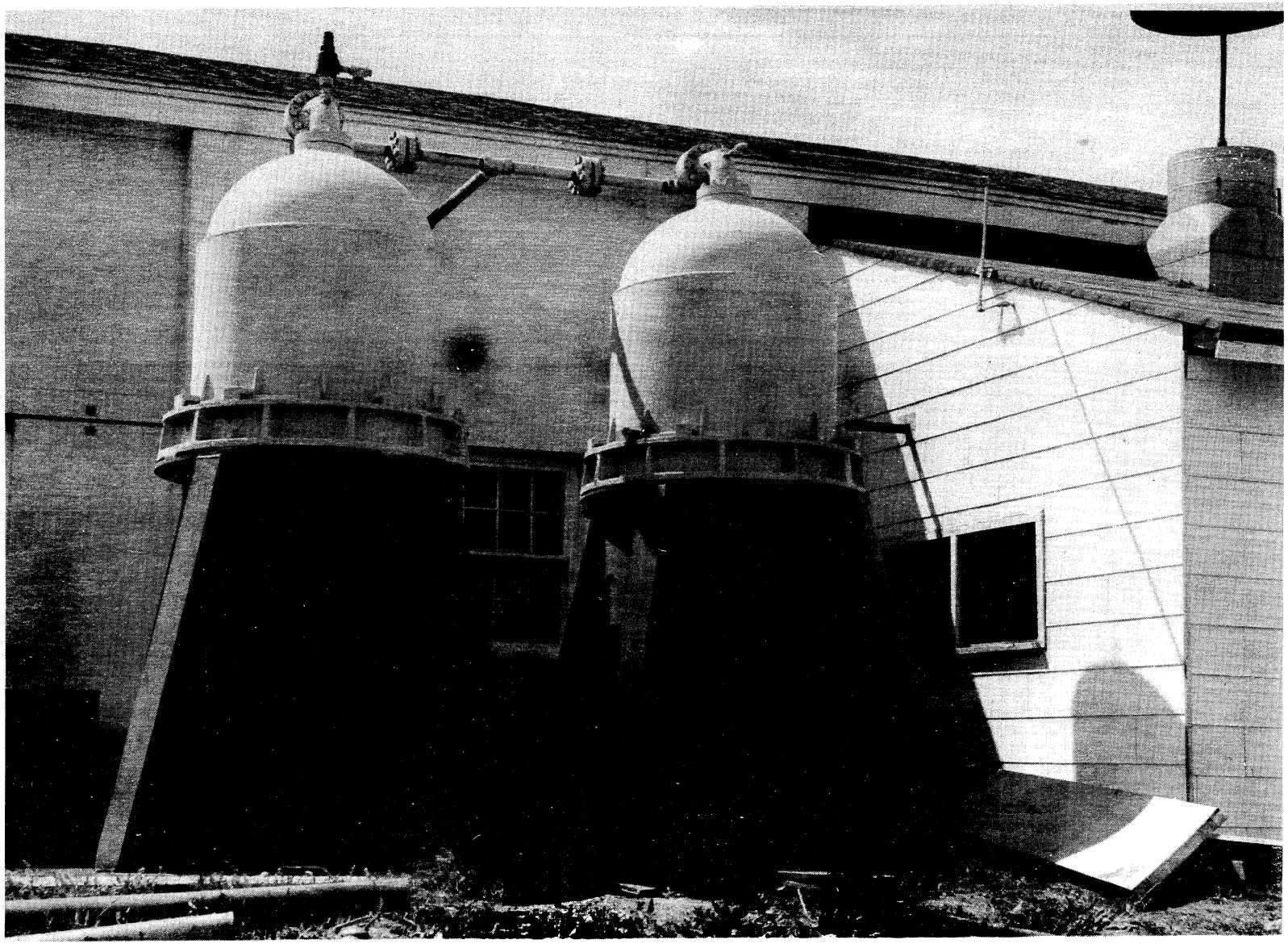

Fig. 2 Photograph of High-pressure Air Storage Tanks

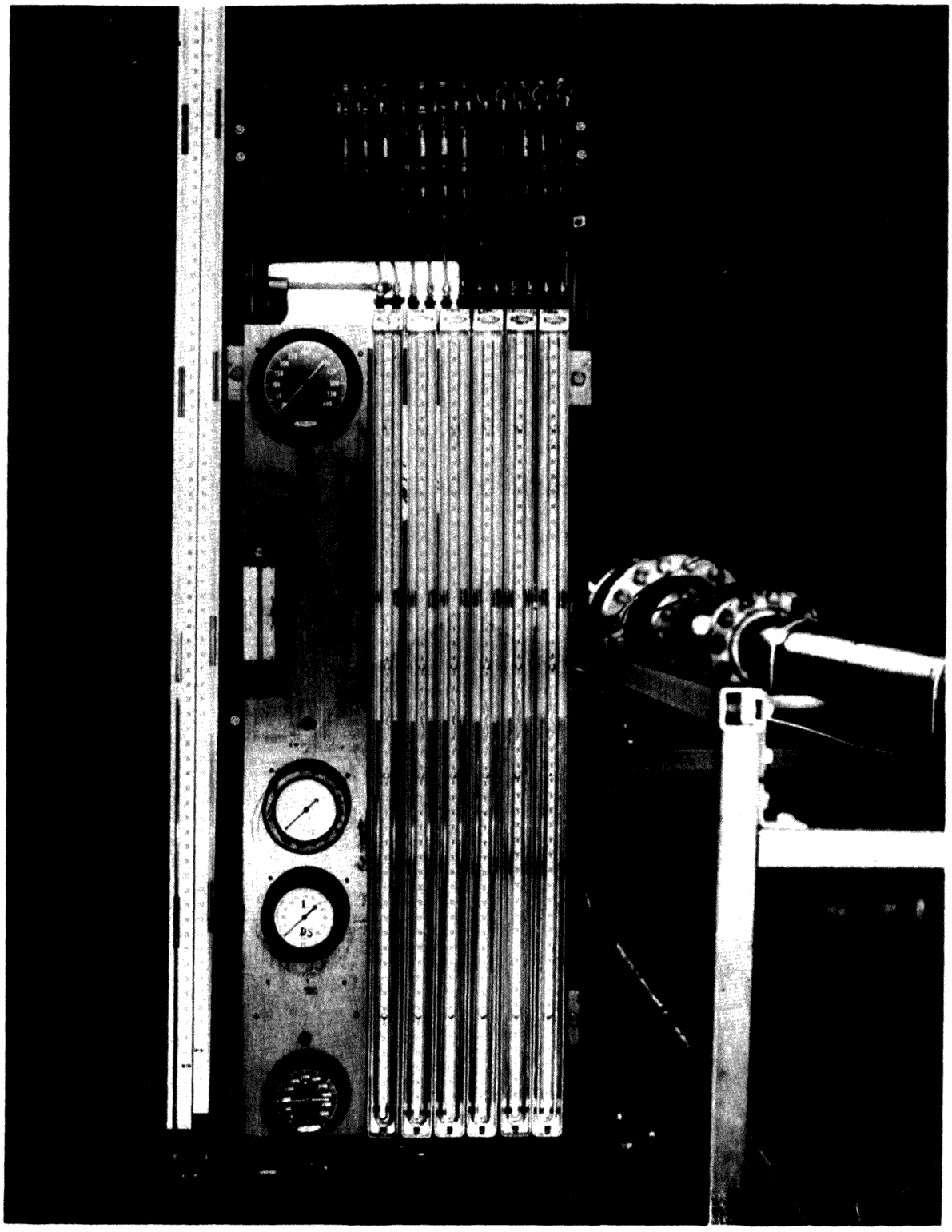

Fig. 3 Photograph of Gauges and Manometer Board
Used in Valve Testings

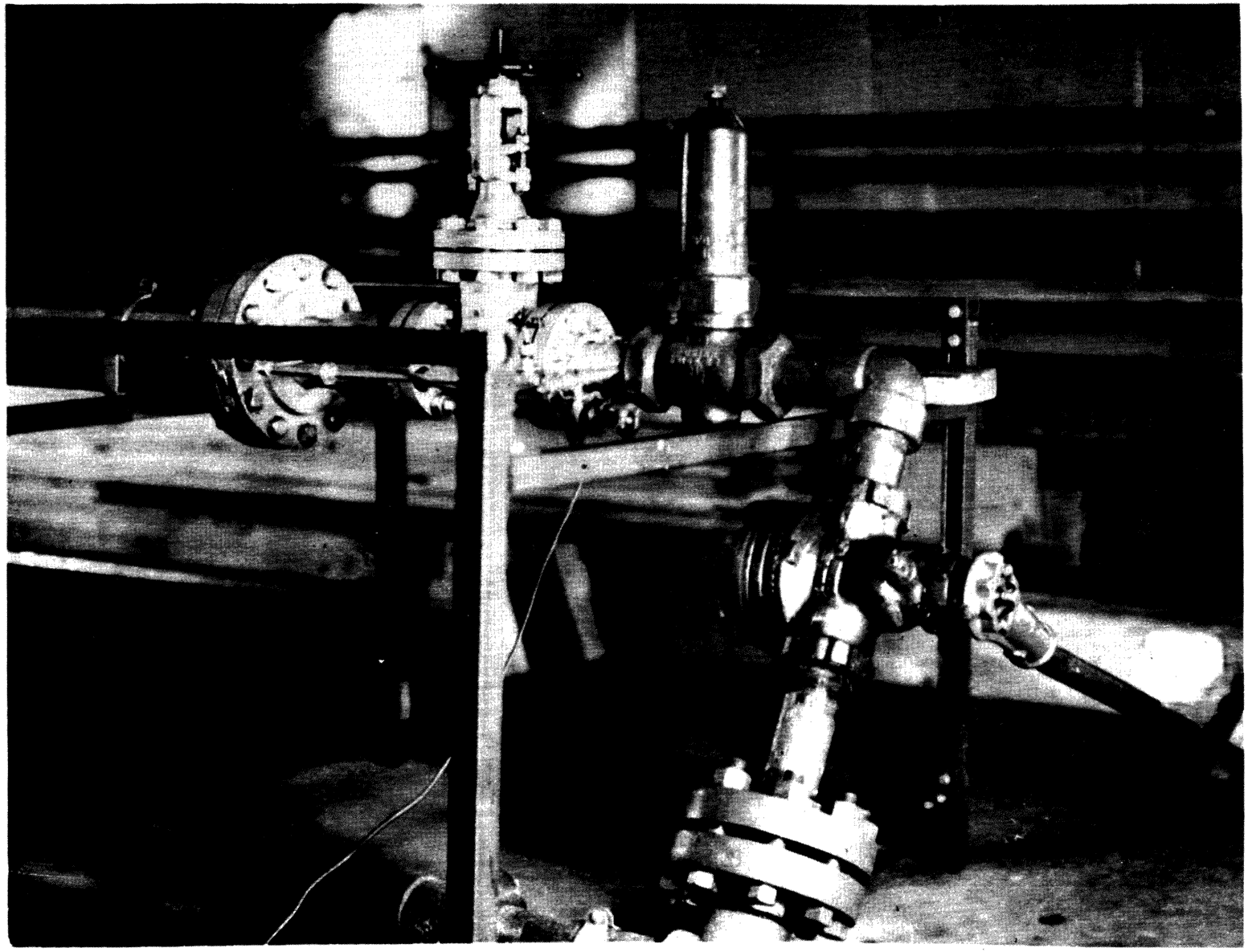

Fig. 4 Photograph of Air Flow Control Valves

The manometer may be read by eye to perhaps 0.02 inches and the photographic data to about 0.05 inches.

Valve Torques

The valve torque is measured from the flexing of a cantilever beam attached to the valve shaft at one end and held at the other end between two knife edges. The flexure of the beam is detected by means of 120-ohm strain gauges cemented to the sides of the beam. A Baldwin SR-4 strain-gauge indicator is used for reading the torque; the system calibrated by means of dead weights hung on the beam (Fig 5). The weights were evaluated on a triple-beam balance. This system will detect a torque of 0.01 ft-lbs and has an accuracy of approximately 1 per cent.

Tank Blowdown Temperatures

The following system was used to measure tank temperatures during blowdown. A special brass plug was made for an opening in the top of the tank. Three thermocouple leads were passed through this plug, cemented into it with molten sulfur. The thermocouple leads were allowed to hang down inside the tank and were of such lengths as to measure the temperatures at the top, at the middle, and near the bottom of the tank. Two other thermocouples were placed on the outside tank wall, one near the top and one near the bottom. These thermocouples were cemented in place on a burnished portion of the tank wall by means of a cement composed of powdered copper mixed with clear lacquer. Qualitative tests show that this cement has good thermal conductivity.

The temperatures of the thermocouples were read from a Brown self-balancing potentiometer modified so as to indicate the temperature range -200°F to +100°F. This instrument was calibrated against a good spirit thermometer using various cold mixtures. The chromel-alumel thermocouples used are very nearly linear in this temperature range. An occasional check was made of the system using a water-ice bath as a reference. At no time was a temperature error indicated greater than 0.5°F from the 32°F reference point.

The tank pressures were measured with a good-quality Bourdon-tube pressure gauge (range 0-5000 lbs). This gauge is claimed by the manufacturer to have an accuracy of 2 per cent of full scale.

It was noted that sunshine on the tank would cause the temperature to be some 20-30°F higher at the top of the tank than at the bottom. For this reason, the data presented in Fig. 11 were taken early in the morning, when the tank temperature was nearly uniform.

Fig. 5 Photograph of Torque-measuring Equipment

Data Recording

It was found convenient at times to record the data photographically. This was done with a 4 x 5 inch Graph View Camera. Typical exposures using four No. 2 Photoflood lamps at 8 ft and Ansco Supreme film were 1/5 sec at f/11. When reading directly from the negative, a certain amount of overexposure has been found helpful.

Pressure Ratio

In general, the term pressure ratio refers to a static pressure ratio. A plot relating upstream total pressure to upstream static pressure is included for each valve, for use when total pressures are desired (Figs. 22 and 33).

II. BLOWDOWN STUDY OF A HIGH-PRESSURE AIR STORAGE TANK

A series of tests was made of a high-pressure air storage tank in order to determine pressure and temperature relations in the tank as a function of blowdown rate. The dimensions of the tank are shown in Fig. 7. The volume of the tanks and adjacent fittings was determined by gravimetric means.

Temperatures were measured at points 1, 2, 3, 4, and 5 in Fig. 7 by means of thermocouples connected to a modified Brown self-balancing potentiometer. The precision of this instrument is about 0.25°F and the accuracy about 0.5°F. An error in the measured air temperature exists due to the lag in the temperature of the thermocouple relative to that of the air surrounding it. This measurement error is discussed in Appendix A.

The temperatures measured at points 1, 2, 3, 4, and 5 are plotted against time on the temperature and pressure charts (Figs. 8-11). Curve No. 6 on these charts shows the temperature of an adiabatic reversible expansion of the air in the tank based on the amount of air discharged in the given time. An average value for k of 1.67 has been taken as representative for the isentropic expansion of air under the given conditions of pressure and temperature. Curve No. 7 (Figs. 8-11) shows tank pressure as a function of blowdown time. The pressure axis is on the right-hand side of the chart. During the tank blowdown, an attempt was made to maintain tank pressure as a linear function of time. For this condition:

$$P_2 = P_1 - bt$$

and using

$$\frac{T_2}{T_1} = \frac{P_2}{P_1}^{(k-1)/k}$$

$$\frac{T_2}{T_1} = \frac{P_1 - bt}{P_1}^{(k-1)/k}$$

then $$T_2 = T_1 \left(1 - \frac{bt}{P_1} \right)^n ,$$

where

P_1 = starting pressure,

T_1 = starting temperature,

P_2 = pressure at any time during the run,

T_2 = air temperature at the time taken for P_2,

k = specific heat ratio,

n = $(k-1)/k$,

b = a constant, and

t = time from start of run.

If the above expression is used to relate T_2 to time, a curve such as a in Fig. 6 is obtained for the isentropic process. The addition of heat during the expansion gives a curve such as b in Fig. 6. This necessarily follows, since heat is added to the air from the relatively warm tank walls.

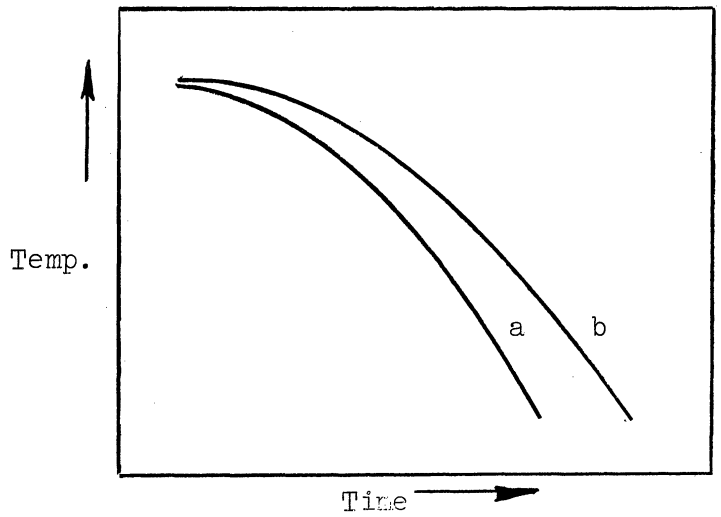

Fig. 6a. Comparison of time-temperature curves for a tank blowdown at constant rate of pressure change: (a) isentropic conditions, (b) with heat addition.

It will be noticed that the shapes of experimental curves are not as regular as the shape of curve b in Fig. 6. The sharp turn up at the start of the No. 2 temperature curve (Figs. 8-11) is due to the accumulation of warm air in the top of the tank. Other irregularities are probably due to the effects of convection currents inside the tank. The humps on the Nos. 1, 2, and 3 curves of Fig. 9 are almost certainly caused by the freezing of supercooled water droplets on the thermocoupled elements. The actual air temperature would follow the dotted lines under the humps in this case (see Fig. 9).

The curves resulting from the blowdown runs are included immediately after this section and are captioned "Temperature and Pressure vs. Time" (Figs. 8-11). These curves show the temperature of the discharged air as it is related to the blowdown rate. In addition to this, the relative approach to an isentropic expansion is shown. The curves for rapid blowdown show the nearest approach to isentropic conditions.

Further examination of the experimental curves established the interesting characteristic that the curves for a high blowdown rate more nearly approach isentropic conditions than the curves for a low blowdown rate. This is to be expected but the degree to which the isentropic conditions are approached is not proportional to the blowdown rate, so that an extremely high rate of blowdown would be necessary to approximate isentropic conditions. As yet sufficient data have not been taken to establish this relationship quantitatively.

The approach to isothermal conditions is controlled by the heat transfer from the tank wall to the air inside the tank. It would be relatively simple to take the data for a run and calculate the effective heat-transfer coefficient for some position of the run, but an attempt to extend this result to all conditions of blowdown amounts to an unjustified extrapolation of the existing correlations of heat transfer.

III. FLOW AND TORQUE CHARACTERISTICS OF A CIRCULAR BUTTERFLY VALVE

The flow characteristics of a 6-inch circular butterfly valve at supercritical pressure ratios have been discussed in an earlier report.* It is the purpose here to extend this work to cover subcritical pressure ratios, and to present information on valve torque and valve plate pressures.

* "Flow Characteristics of a Butterfly Valve at Supercritical Pressure Ratios", by L. C. Garby, J. S. Murphy, H. H. Hicks, Jr., University of Michigan, Engineering Research Institute, 15 June 1951.

In the earlier report on the 6-inch circular valve, it was shown that a flow coefficient could be defined for the valve. This flow coefficient (C_f) was based on the experimental mass flow through the valve divided by the computed mass flow, assuming a straight sonic line at the valve opening. C_f was shown to be essentially independent of valve angle and pressure ratio in the supercritical flow region. The computed mass flow was based on the projected opening of the valve, which in this case is given by:

$$A_\beta = A_o (1-\cos \beta) \quad ,$$

where

A_o = area of the valve duct with the valve plate removed, and
β = valve angle measured from the closed position.

There is an error in the opening computed in this manner which varies from an amount equal to the cross-sectional area of the valve plate in the fully open position to an amount equal to the projected area of the valve lip near the closed position. This error approaches zero as the valve angle approaches zero (see Appendix C). One difficulty with this method of computing the valve opening lies in the fact that, for small valves of β, the calculated opening A_β is very sensitive to changes in β. A small error in the valve setting or in the indexing on the shaft thus gives rise to large errors in the flow coefficient. For this reason the coefficients are not realistic for angles much less than 15°, and it is now apparent that the small valve angles should be calculated from a clearance measurement.

It has been decided to continue the use of the flow coefficient term C_f that was presented in the earlier report on supercritical pressure ratios; the data for the subsonic case are presented in this report on the C_f basis.

It was mentioned in the summary that the method of computing the mass flow for subcritical pressure ratios could no longer assume a straight sonic line at the valve opening. The mass flow for the subcritical case is calculated assuming the flow into the valve opening to be isentropic. The Mach Number in the opening is then given by

$$M = \sqrt{\frac{2}{k-1} \left(r^{-(k-1)/k} - 1\right)} \quad .$$

The temperature in the opening is given by

$$T = T_o \, r^{(k-1)/k} \quad .$$

The air density in the opening is given by

$$\rho = \rho_o \, r \, \frac{T}{T_o}$$

where

$$r = P_2/P_o \quad .$$

From these values, the mass flow through the opening is computed to be

$$Q = \rho AV \quad .$$

The pressure P_2 used above is the wall static pressure measured immediately downstream of the valve. P_2 should be the static pressure in the valve opening. A check at high mass flow showed only a negligible difference in the two pressures, and therefore the downstream pressure is satisfactory.

It will be noted that there is considerable scatter in the experimental valves of the flow coefficient C_f in the subsonic range. This scatter is partly due to valve clearance, which causes the actual valve opening to be larger than the opening calculated from the valve angle. The scattering caused by clearance is most noticeable at small angles (5° and 10°). Also contributing to the scatter at low angles are errors in the valve angle setting. The scatter at large valve angles is due primarily to errors in the flow measurement. The orifice plates which were used to measure the flow could not be calibrated reliably for the measurement of large mass flows at low absolute pressures (see Appendix B). The average value of the flow coefficient C_f for the circular valve is about 0.70 for a pressure ratio of 1.0 and increases to a value of about 0.90 for pressure ratios of 2.0 or greater. Further work using an improved flow-measuring technique is necessary to define the flow coefficient more accurately (Figs. 23 and 24). It should also be noted that the wide variation in Reynolds Number may affect the flow stability and therefore the flow coefficient.

The valve torque is presented as a function of valve angle and pressure ratio. The peak torque occurs at an angle of about 70° for all the pressure ratios studied (Figs. 20 and 21).

In order to nondimensionalize the torque data and to present it in the form of a torque coefficient (C_f), it is necessary to divide the measured torque by a quantity having the dimensions of torque. If the coefficient thus determined is to provide any generalization of the data, then the terms that are used to nondimensionalize the torque must in some way determine the torque.

For instance, the following terms may be used to nondimensionalize the torque.

$$C_f = \frac{\text{Measured torque}}{\text{pressure x area x length}}$$

It is now necessary to determine whether the quantity (pressure x area x length) can be developed from a consideration of the valve flow and geometry.

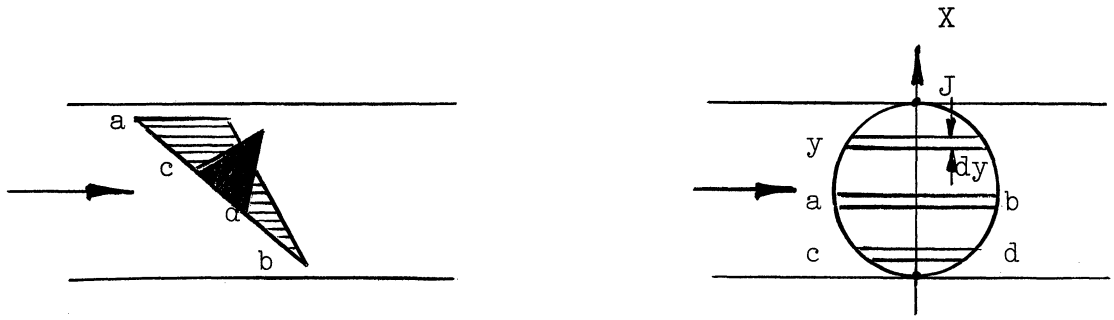

Part I Part II

Fig. 6b

Parts I and II of Fig. 6b represent flow through a circular butterfly valve. Take an arbitrary distribution of net pressure across chord ab. This is shown as the light shaded area in Part I. This pressure distribution is assumed to hold for some given values of pressure ratio and valve angle. The assumption is now made that whatever the pressure distribution may be across chord ab, the same pressure distribution exists, in per cent of chord, across chord cd. This is represented by the dark shaded area in Part I, This assumption is based more on experimental observation than on theoretical considerations, which indicate that the pressure distribution should be a function of a Reynolds Number. The Reynolds Number might be based on the chord length or on the distance from the end of the chord to the valve wall.

It is probable that there would be a Reynolds Number effect for geometrically similar valves of different sizes. This would particularly be expected for large valve angles, where separations must occur.

Until a correlation based on the Reynolds Number can be made, it is felt that the assumption of similar pressure distribution across chords of different length is reasonable and represents the facts to a moderate degree of accuracy. The torque on the valve may now be evaluated on the basis of the preceding assumptions.

The force on any chord element of length y and width dx is

$$dF = Pn_1 \, y \, dx \quad .$$

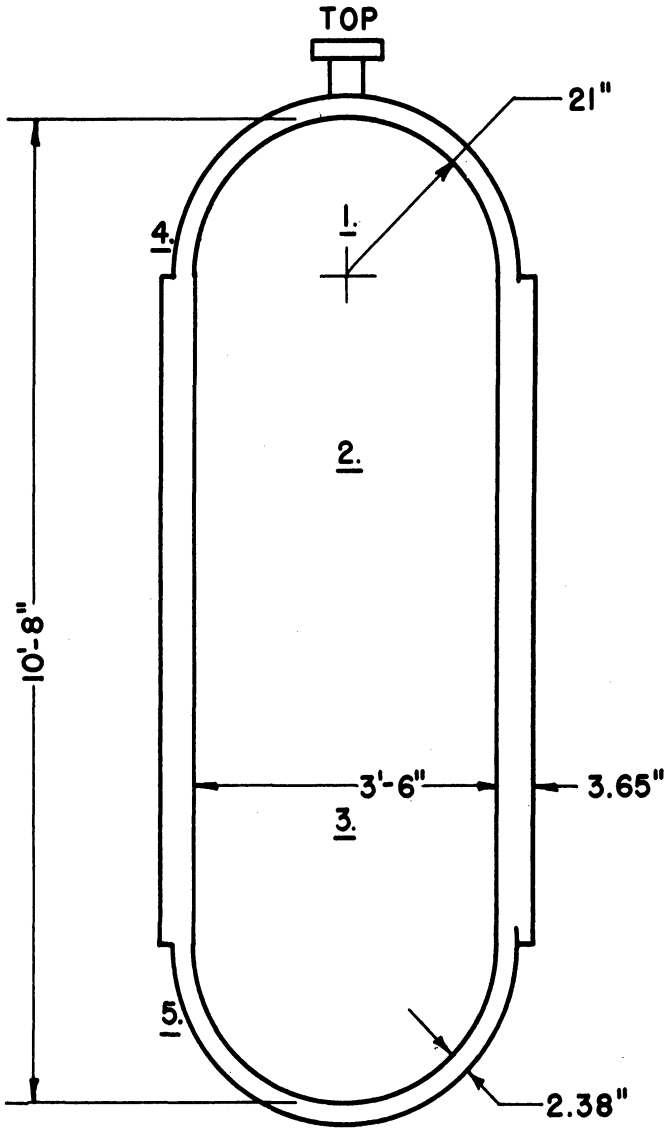

DATA: STEEL PRESSURE TANK
SPECIFICATION WEIGHT - 21,000 LBS
MEASURED VOLUME - 85.12 CU. FT.
TEMPERATURE - MEASURED AT POINTS 1,2,3,4,5
SCALE: 1/2" TO 1'
WORKING PRESSURE - 3,500 P.S.I.

AWS

FIG. 7.

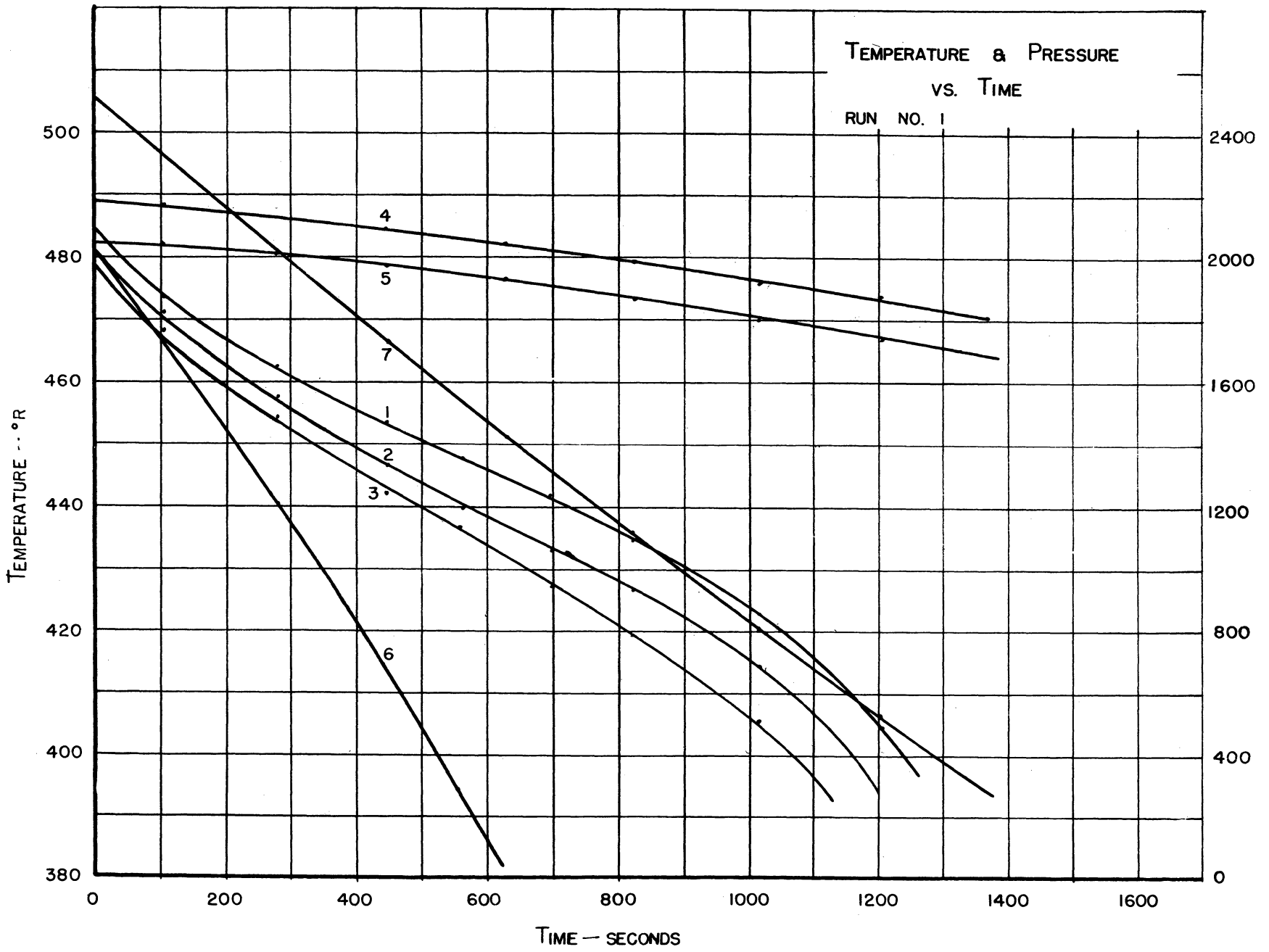
TEMPERATURE & PRESSURE
VS. TIME
RUN NO. 1
TEMPERATURE -- °R
PRESSURE— PSIA. (Curve No. 7)
TIME — SECONDS
500
480
460
440
420
400
380
2400
2000
1600
1200
800
400
0
0
200
400
600
800
1000
1200
1400
1600
1
2
3
4
5
6
7

FIG. 8

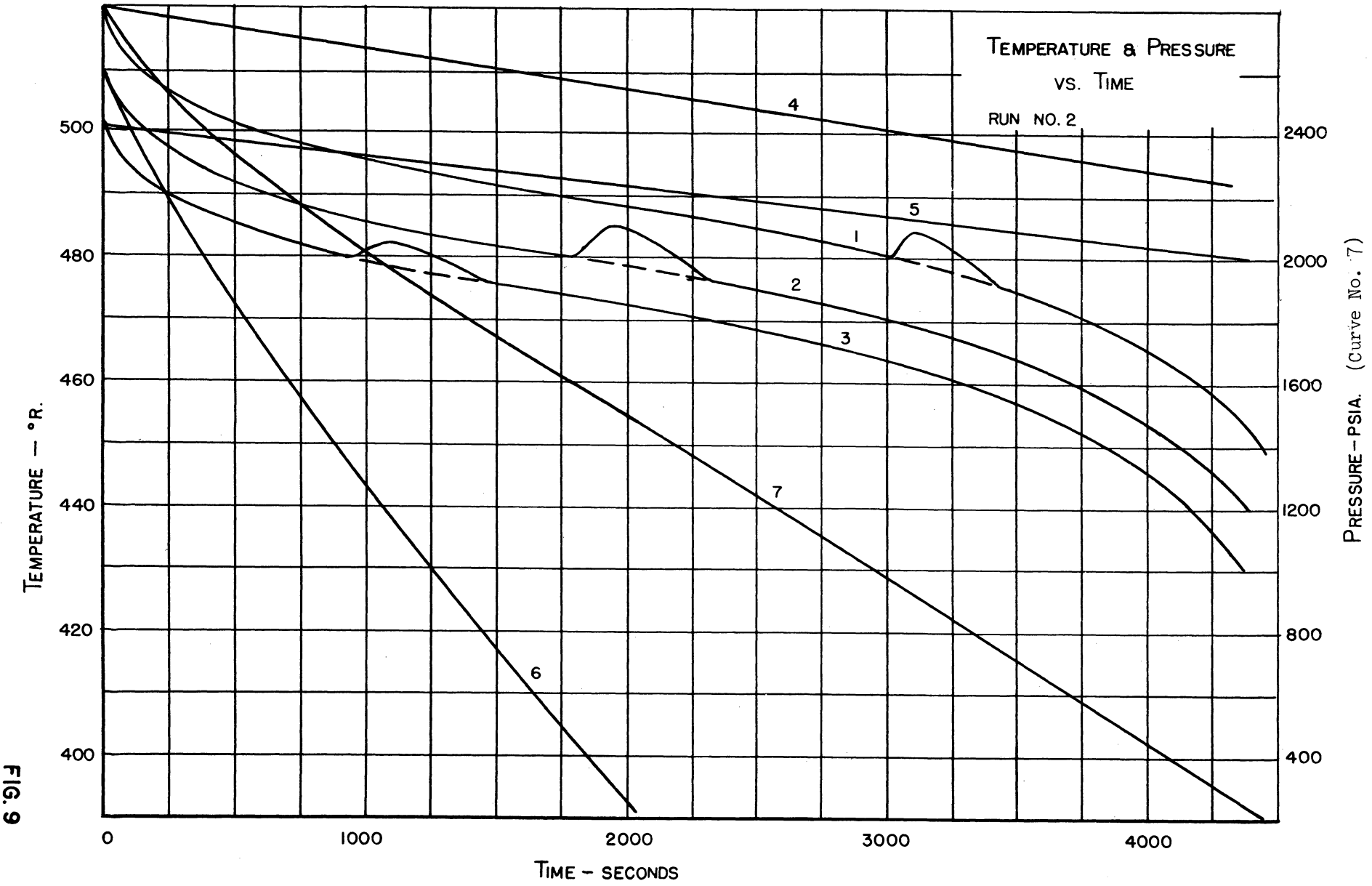
TEMPERATURE & PRESSURE
VS. TIME
RUN NO. 2
TEMPERATURE – °R.
PRESSURE – PSIA. (Curve No. 7)
TIME – SECONDS
500
480
460
440
420
400
2400
2000
1600
1200
800
400
0
1000
2000
3000
4000
1
2
3
4
5
6
7

FIG. 9

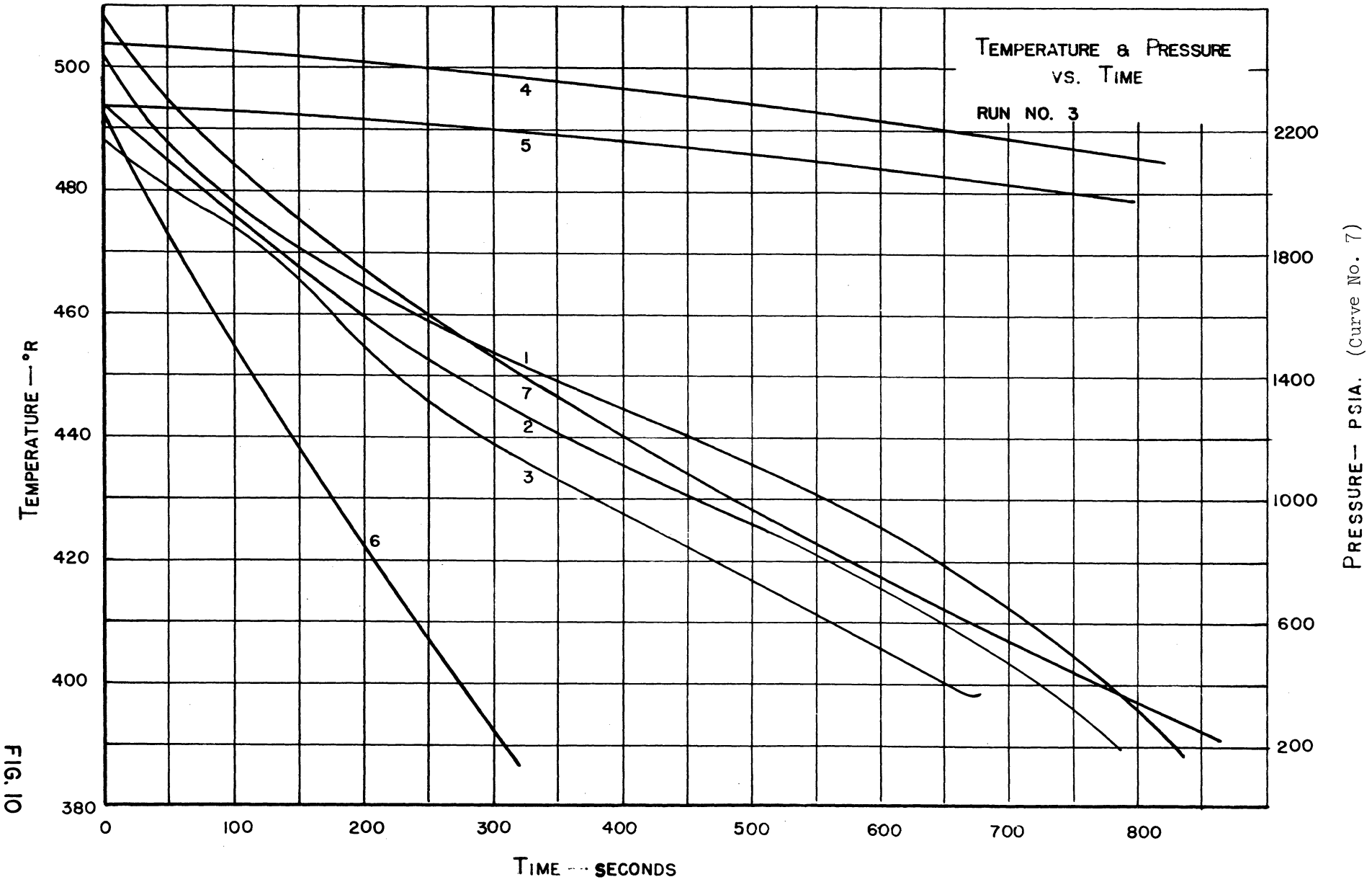
TEMPERATURE & PRESSURE
VS. TIME
RUN NO. 3
TEMPERATURE — °R
PRESSURE— PSIA. (Curve No. 7)
TIME --- SECONDS
500
480
460
440
420
400
380
2200
1800
1400
1000
600
200
0
100
200
300
400
500
600
700
800
1
2
3
4
5
6
7

FIG. 10

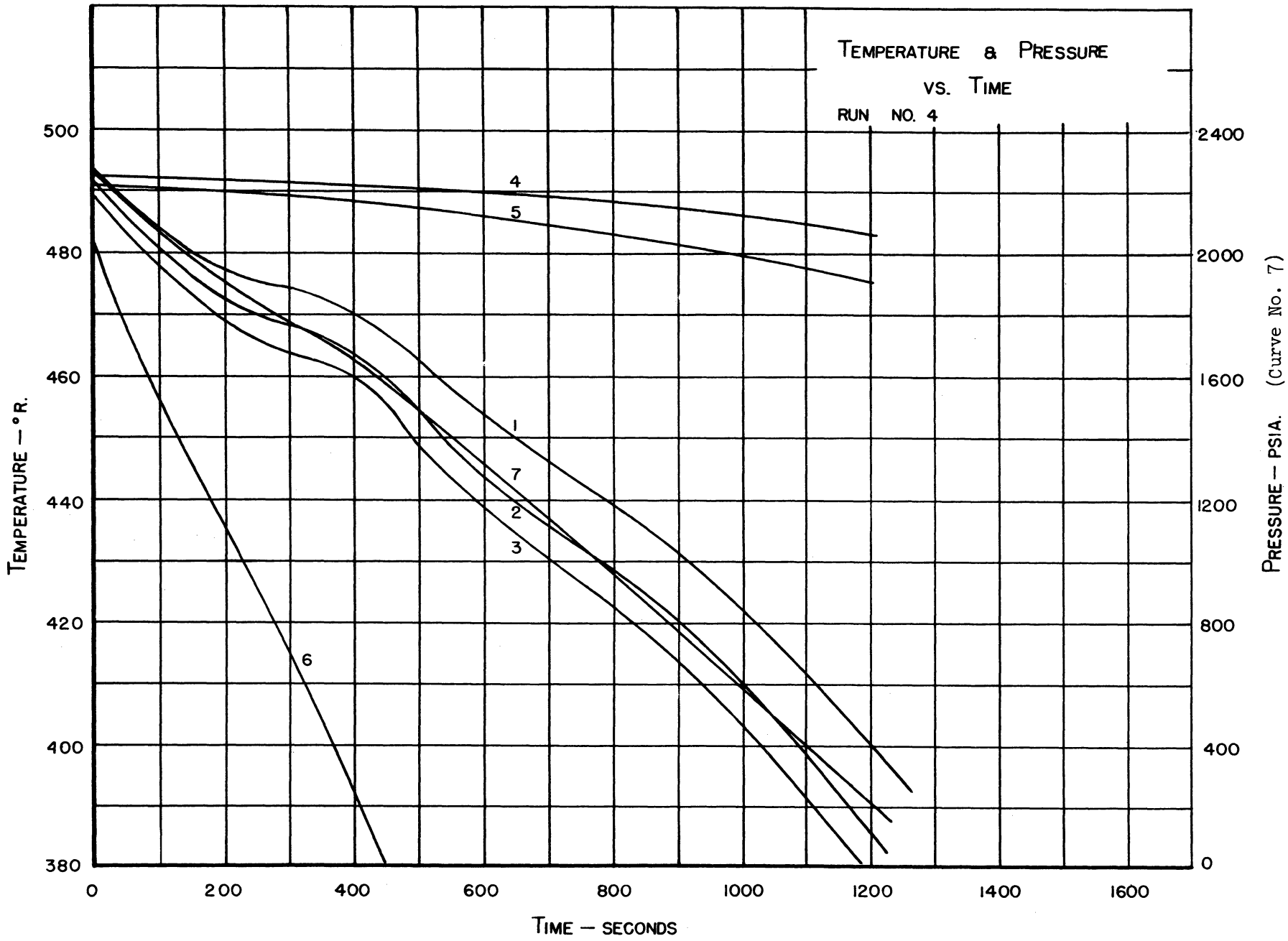
TEMPERATURE & PRESSURE
VS. TIME
RUN NO. 4
TEMPERATURE — °R.
PRESSURE — PSIA. (Curve No. 7)
TIME — SECONDS
500
480
460
440
420
400
380
2400
2000
1600
1200
800
400
0
0
200
400
600
800
1000
1200
1400
1600
1
2
3
4
5
6
7

FIG. 11

The torque about the valve axis due to the force dF is

$$dT = dF\, n_2 y$$

$$dT = Pn_1 n_2\, y^2 dx = Pn_3\, y^2 dx$$

$$T = Pn_3 \int_0^J y^2 dx,$$

where

P = a reference or datum pressure,

n_1 = a constant determined by the pressure distribution,

n_2 = a moment-arm proportionality constant, also determined by the pressure distribution, and

T = valve torque.

The integration indicated above, if carried out for a circular value, gives the result,

$$T = \frac{16}{3}\, Pn_3\, J^3 ,$$

where J is the diameter of the circle. It is seen that the integration has the dimension of pressure x area x length and will nondimensionalize the measured torque. The torque coefficient for the circular valve then becomes

$$C_t' n_3 = C_t = \frac{\text{Measured torque}}{16/3\ P_o\ J^3} ;$$

for the 6-inch circular valve,

$$C_t = \frac{\text{Measured torque}}{0.0375\ P_b} .$$

A similar analysis for a 60° segmental valve gives

$$C_t' n_3 = C_t = \frac{\text{Measured torque}}{0.51\ P_o\ J^3} ,$$

when J = valve span;

for the valve tested, $C_t = \frac{\text{Measured torque}}{0.0385\ P_o}$.

For a rectangular valve

$$C_t\ n_3 = C_t = \frac{\text{Measured torque}}{B^2\ P_o\ J} ,$$

when B is the valve chord and J is the valve span;

for the valve tested, $C_t = \frac{\text{Measured torque}}{0.0104\ P_o}$

The torque coefficients are plotted vs valve angle in Figs. 32a and 32b. Pressure ratio is used as a parameter.

There is a fair correlation in the values of C_t for the circular and segmental valves, and some correlation is shown by C_t for the rectangular valve. It cannot be said, however, that this offers any proof of the assumption regarding pressure distribution across the chord.

An interesting characteristic is shown by the pressure ratio parameters. The indication is that for pressure ratios much above 2.0 the torque coefficient is no longer a function of pressure ratio. This might be expected, since at higher pressure ratios the shock waves would move further down the channel and the torque would then depend primarily on the absolute pressure and on the valve angle.

A complete interpretation of the valve plate pressures (Figs. 14-19) will probably have to be done with the aid of optical measurements made on the flow pattern in the valve. An interesting behavior is shown, however, by the plate edge pressure P_{v3} at the angle of 5° (Figs. 16 and 19). If the valve were perfectly symmetrical in construction, it would be expected that the curve for tap configuration A would be the same as that for configuration B (Fig. 13). The pressure tap P_{v3} is not located symmetrically on the edge of the valve plate, however, but is offset to one side so that when the valve is in configuration A the hole is on the upstream side of the plate edge. When the valve is in configuration B, the hole is on the downstream side of the plate edge. When set at 5°, the valve has a small clearance, and the vena contracta of the flow is apparently formed in between the two possible positions (A or B) for the pressure tap P_{v3} . It will be noted from the graphs of P_{v3}/P_2 (Figs. 16 and 19) that for configuration A, the pressure at P_{v3} behaves as though it were above the vena contracta, and for configuration B, the pressure at P_{v3} behaves as though it were below the vena contracta. Furthermore, it is apparent from the shape of the curves that the vena contracta moves relative to pressure tap P_{v3} when the pressure ratio changes. The same behavior is shown to a lesser extent at a valve angle of 10°.

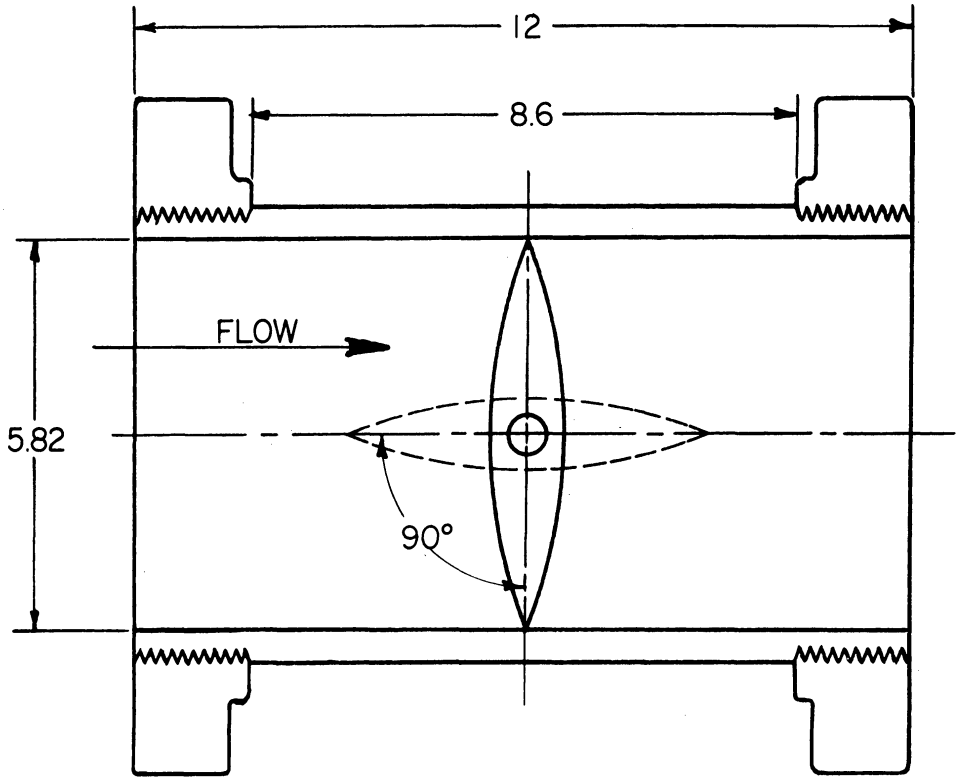

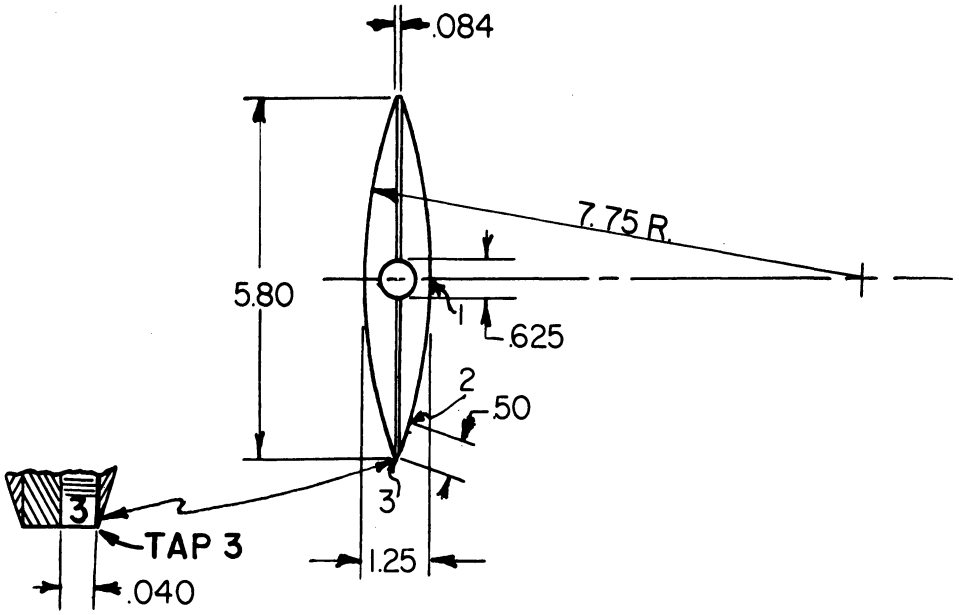

BUTTERFLY VALVE ASSEMBLY – HENRY PRATT – MODEL TI.14 A

SHOWING PRESSURE – TAP LOCATIONS

FIG. 12

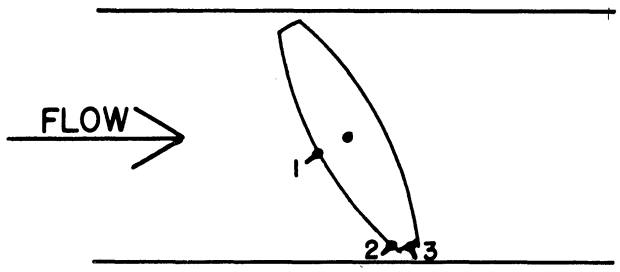

CONFIGURATION "A"

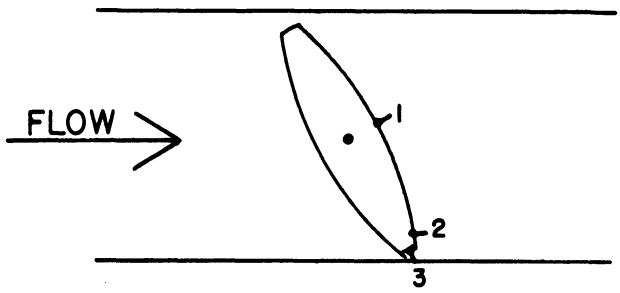

CONFIGURATION "B"

LOCATION OF PRESSURE TAPS
ON VALVE PLATE

AWS

FIG. 13

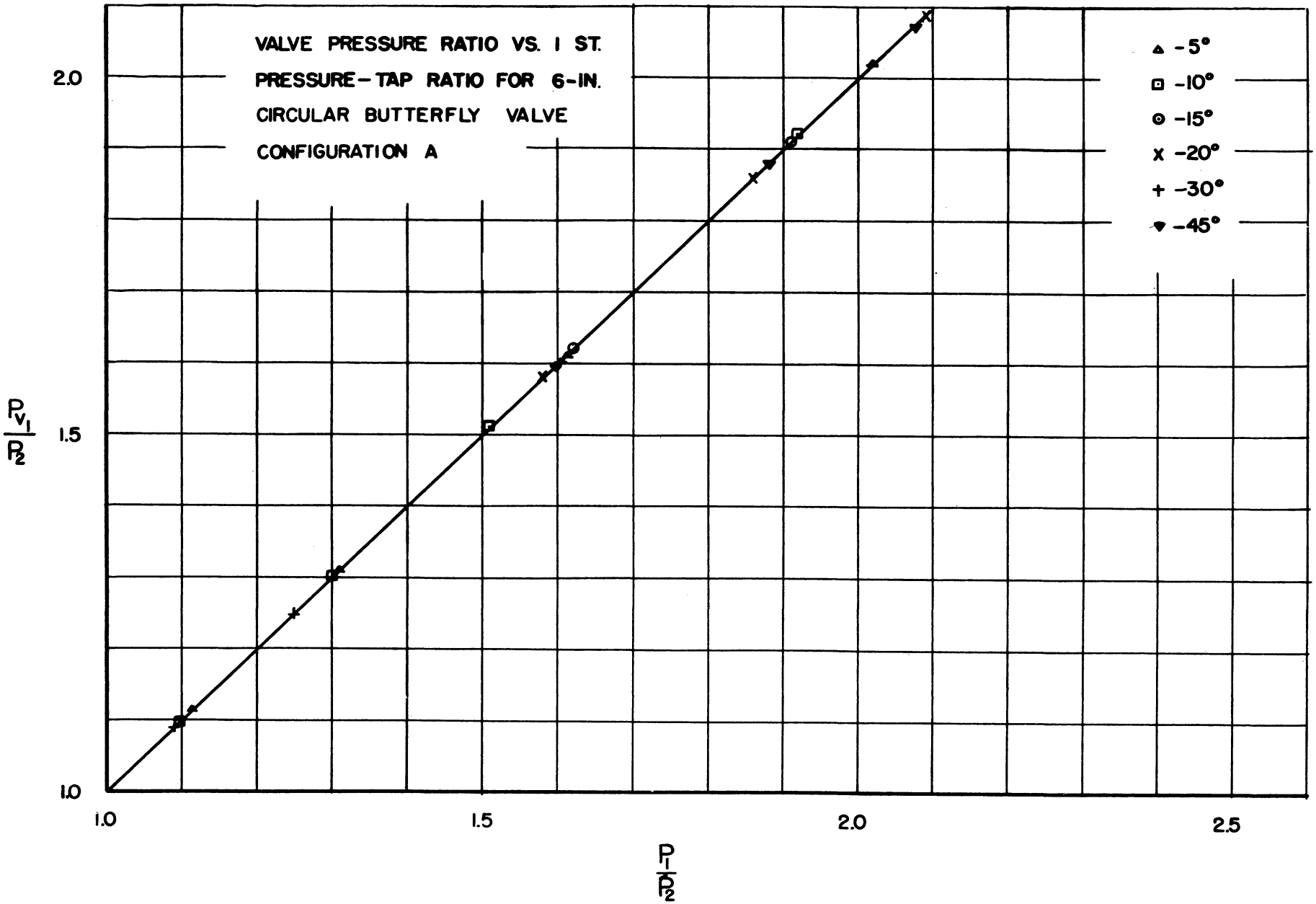
VALVE PRESSURE RATIO VS. 1 ST. PRESSURE-TAP RATIO FOR 6-IN. CIRCULAR BUTTERFLY VALVE CONFIGURATION A
-5°
-10°
-15°
-20°
-30°
-45°
2.0
1.5
1.0
1.0
1.5
2.0
2.5
$\frac{P_{V1}}{P_2}$
$\frac{P_1}{P_2}$

FIG. 14

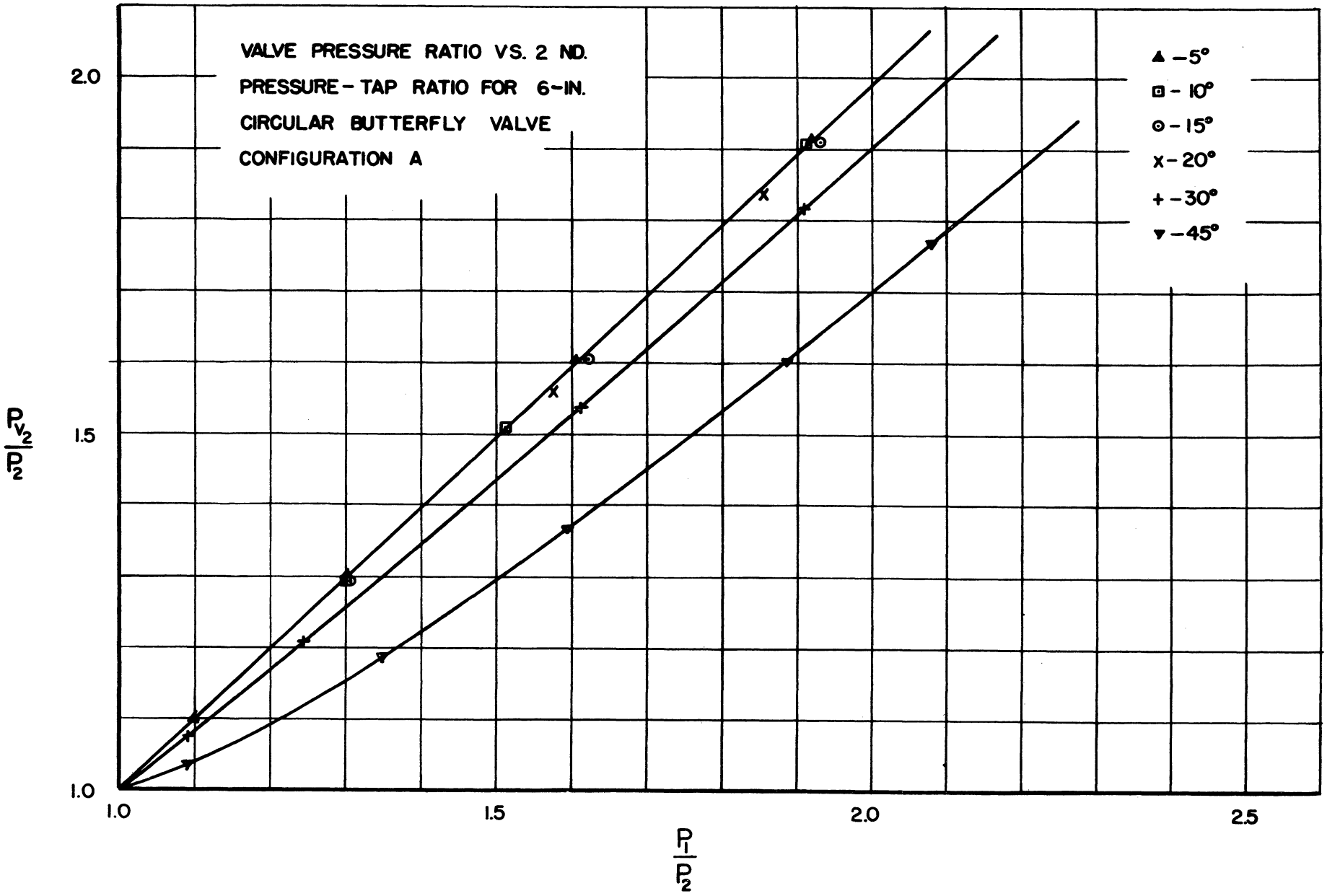
VALVE PRESSURE RATIO VS. 2 ND. PRESSURE-TAP RATIO FOR 6-IN. CIRCULAR BUTTERFLY VALVE CONFIGURATION A
▲ -5°
▣ - 10°
⊙ - 15°
x - 20°
+ -30°
▼ -45°
2.0
1.5
1.0
1.0
1.5
2.0
2.5
$\frac{P_{v_2}}{P_2}$
$\frac{P_1}{P_2}$

FIG. 15

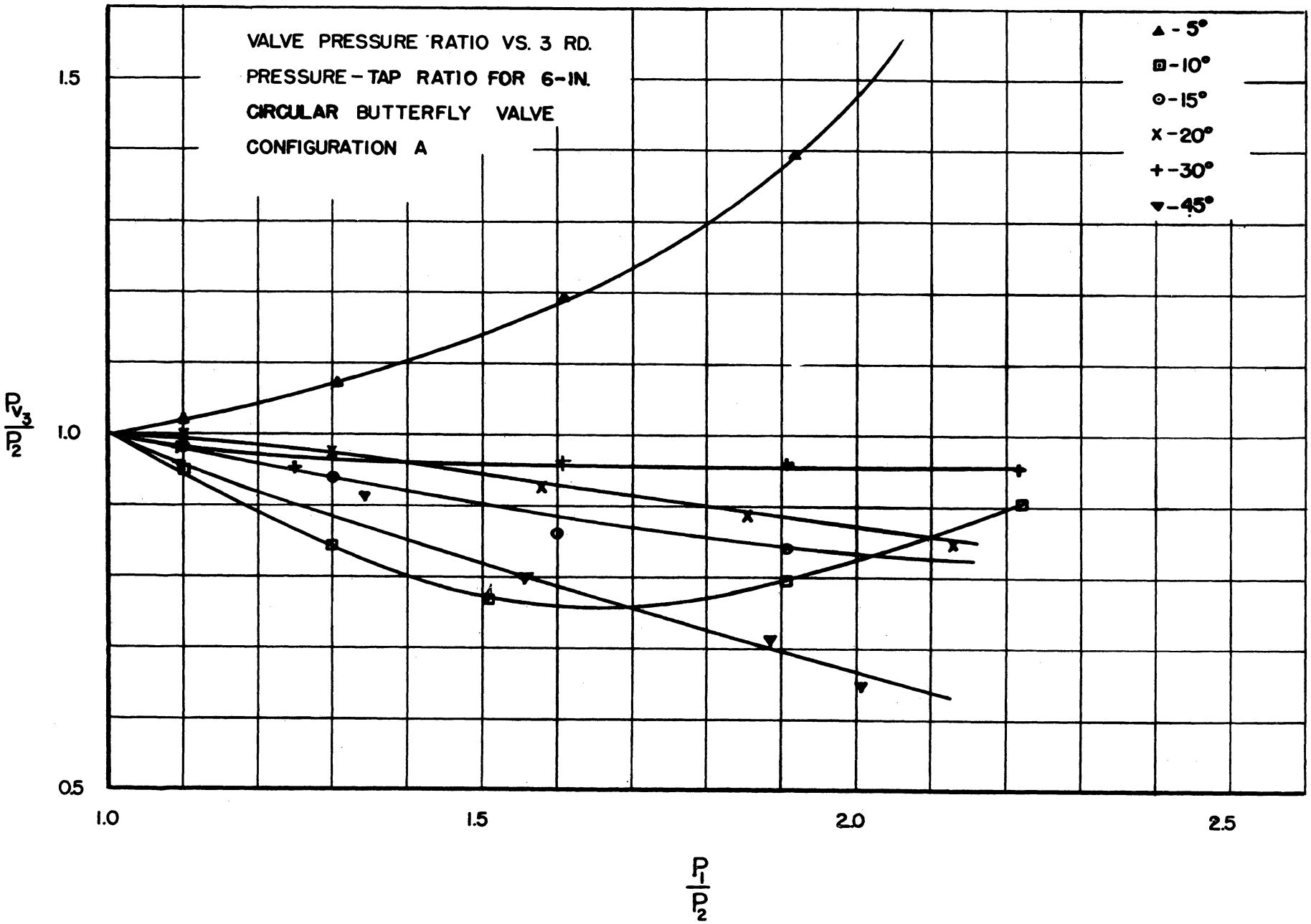
VALVE PRESSURE RATIO VS. 3 RD.
PRESSURE-TAP RATIO FOR 6-IN.
CIRCULAR BUTTERFLY VALVE
CONFIGURATION A
▲ - 5°
⊡ - 10°
⊙ - 15°
x - 20°
+ - 30°
▼ - 45°
1.5
1.0
0.5
$\frac{P_{V_3}}{P_2}$
1.0
1.5
2.0
2.5
$\frac{P_1}{P_2}$

FIG. 16

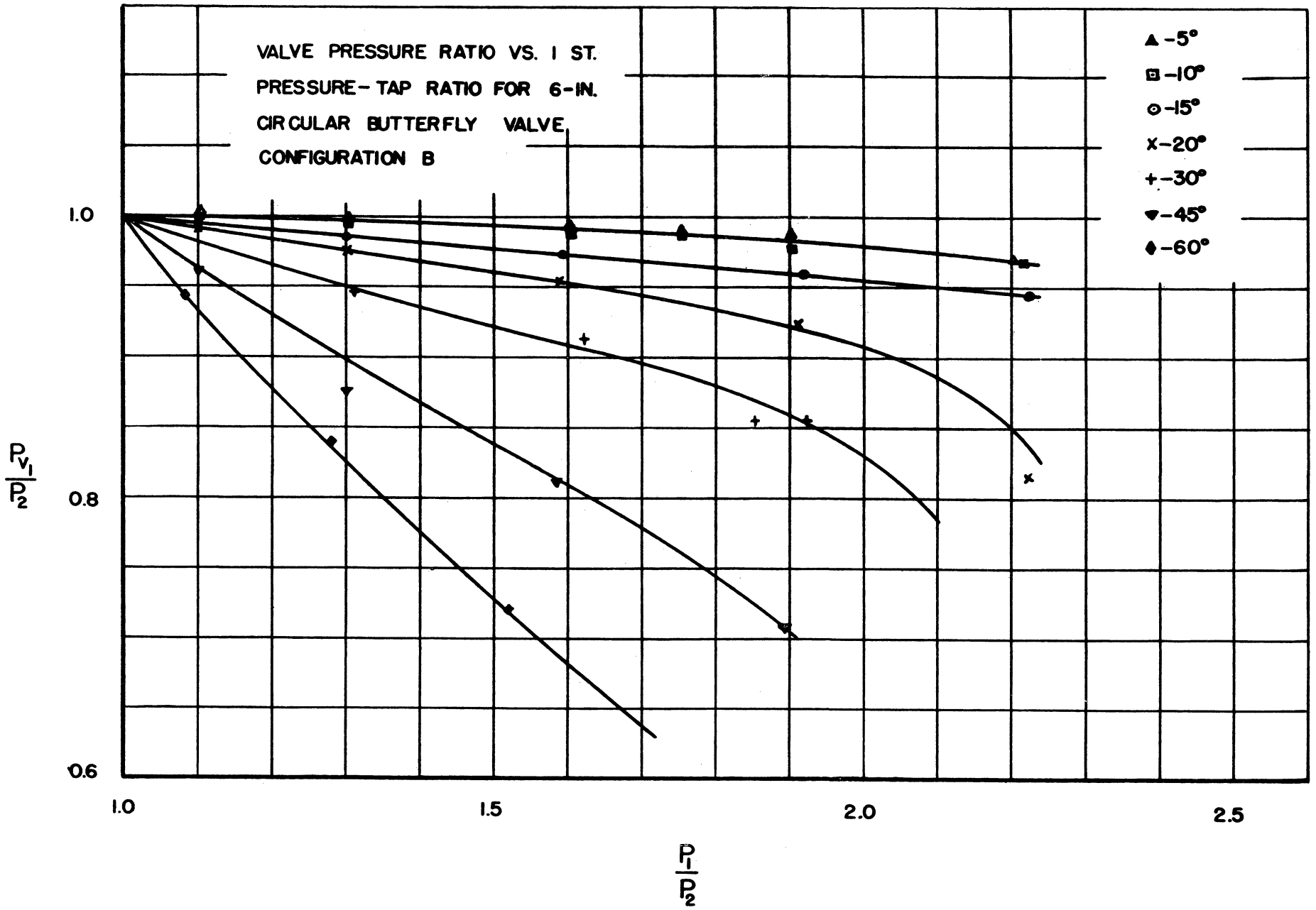
VALVE PRESSURE RATIO VS. 1 ST.
PRESSURE-TAP RATIO FOR 6-IN.
CIRCULAR BUTTERFLY VALVE,
CONFIGURATION B
▲ -5°
⊡ -10°
⊙ -15°
x -20°
+ -30°
▼ -45°
♦ -60°
1.0
0.8
0.6
P_{V_1}/P_2
1.0
1.5
2.0
2.5
P_1/P_2

FIG. 17

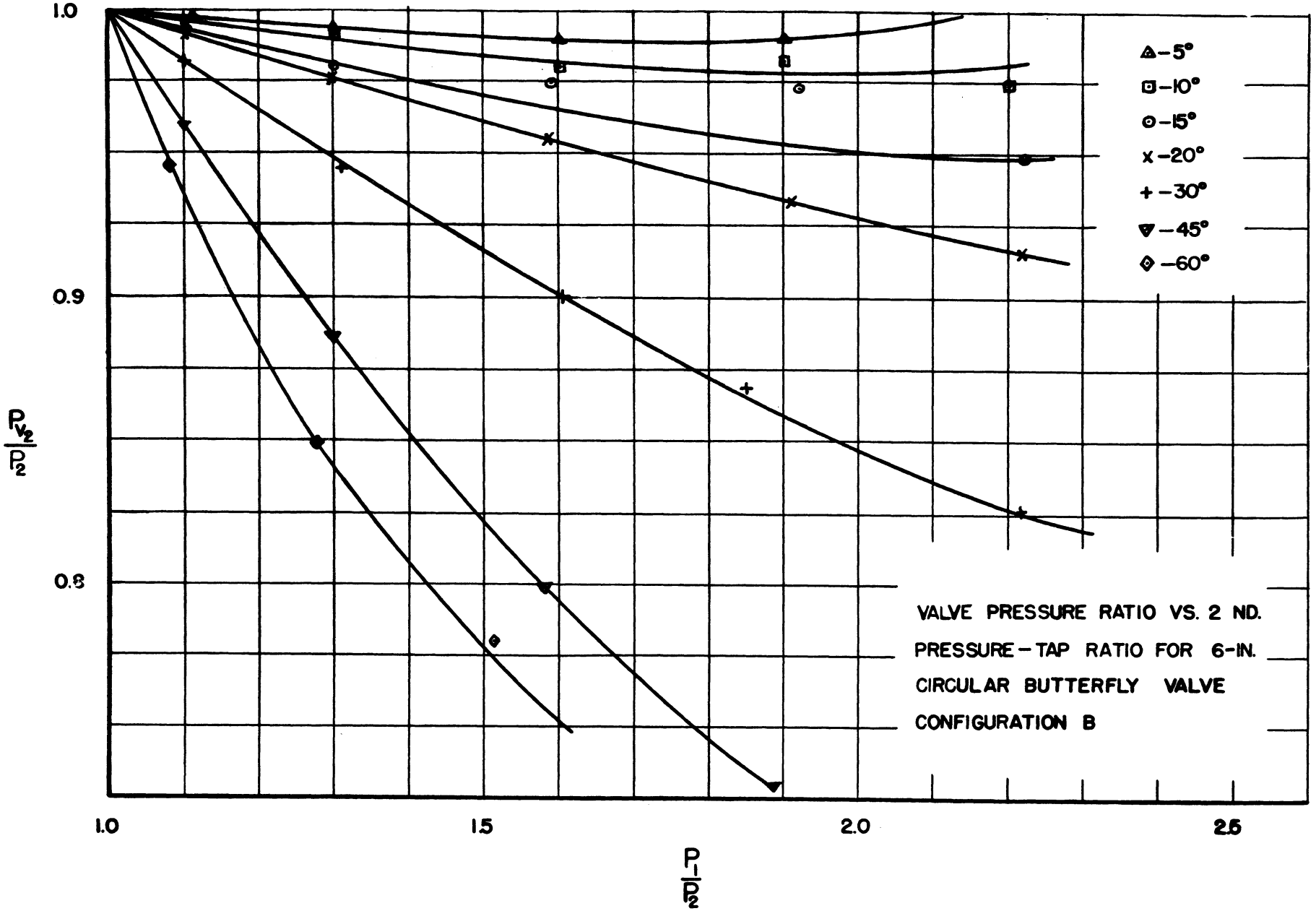
1.0
0.9
0.8
1.0
1.5
2.0
2.5
$\frac{P_{v2}}{P_2}$
$\frac{P_1}{P_2}$
-5°
-10°
-15°
-20°
-30°
-45°
-60°
VALVE PRESSURE RATIO VS. 2 ND.
PRESSURE-TAP RATIO FOR 6-IN.
CIRCULAR BUTTERFLY VALVE
CONFIGURATION B

FIG. 18

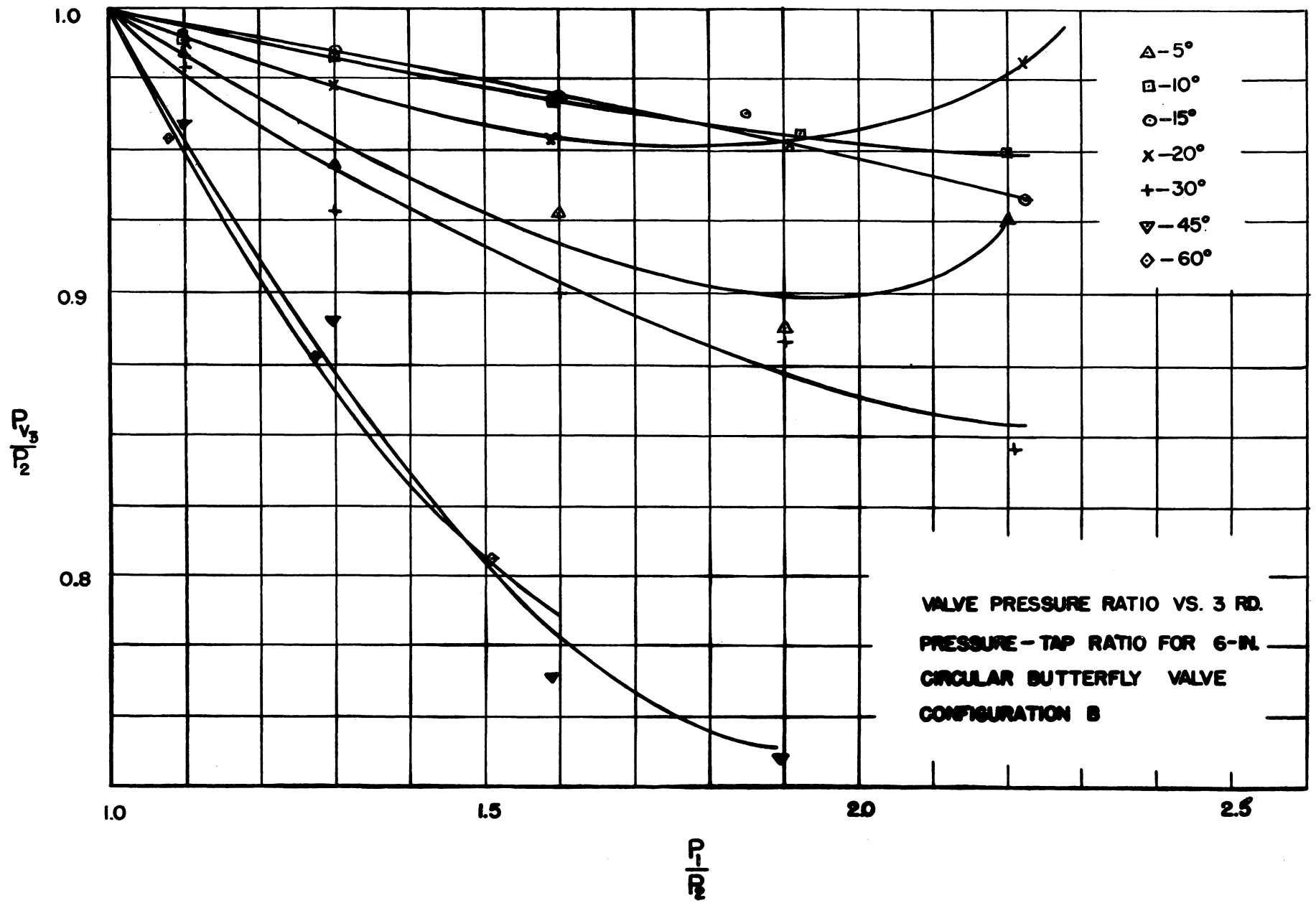
1.0
0.9
0.8
1.0
1.5
2.0
2.5
$\frac{P_{V3}}{P_2}$
$\frac{P_1}{P_2}$
△ – 5°
□ – 10°
○ – 15°
X – 20°
+ – 30°
▽ – 45°
◇ – 60°
VALVE PRESSURE RATIO VS. 3 RD. PRESSURE – TAP RATIO FOR 6-IN. CIRCULAR BUTTERFLY VALVE CONFIGURATION B

FIG. 19

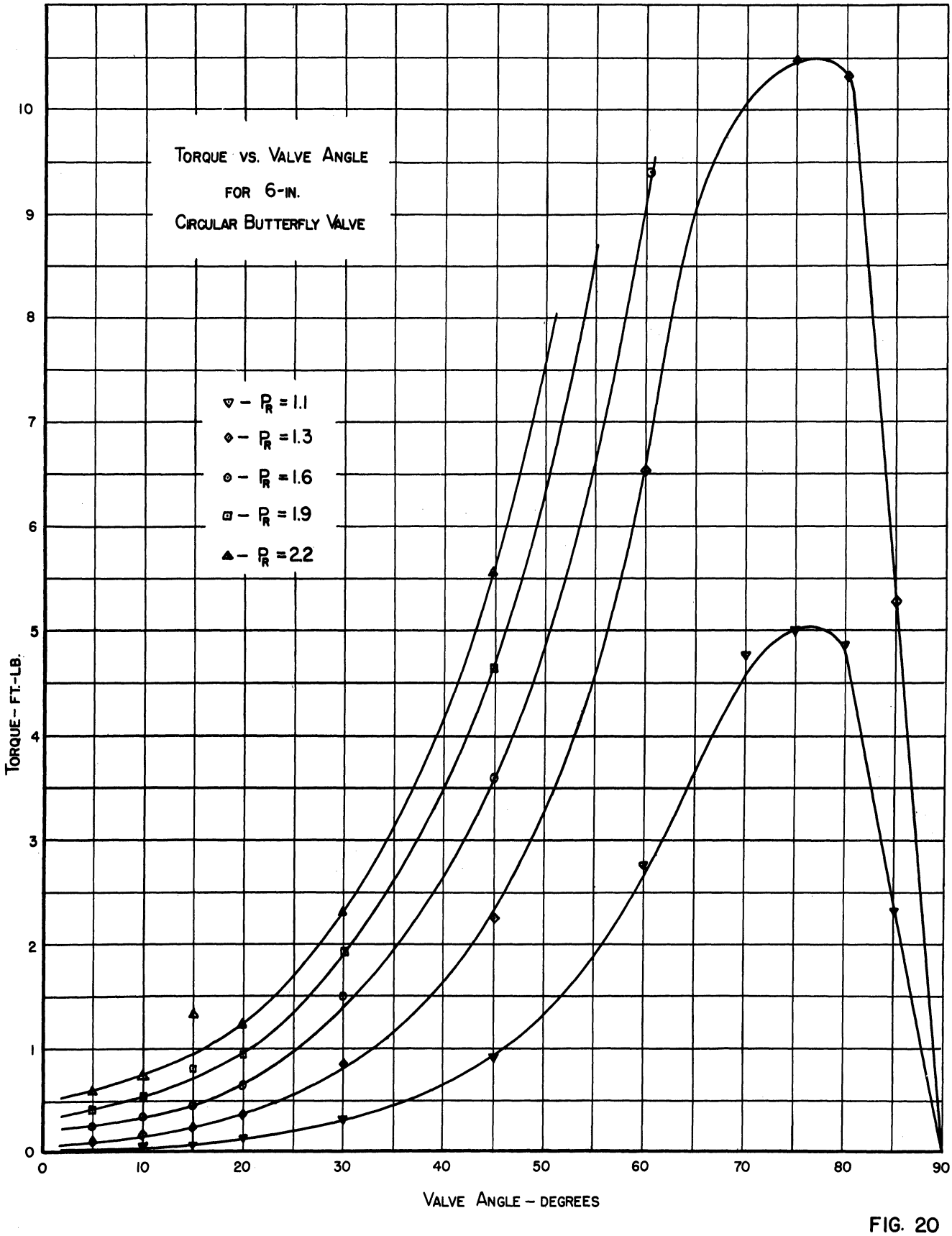
TORQUE VS. VALVE ANGLE
FOR 6-IN.
CIRCULAR BUTTERFLY VALVE
▽ – P_R = 1.1
◇ – P_R = 1.3
○ – P_R = 1.6
□ – P_R = 1.9
△ – P_R = 2.2
TORQUE – FT.-LB.
0
1
2
3
4
5
6
7
8
9
10
0
10
20
30
40
50
60
70
80
90
VALVE ANGLE – DEGREES

FIG. 20

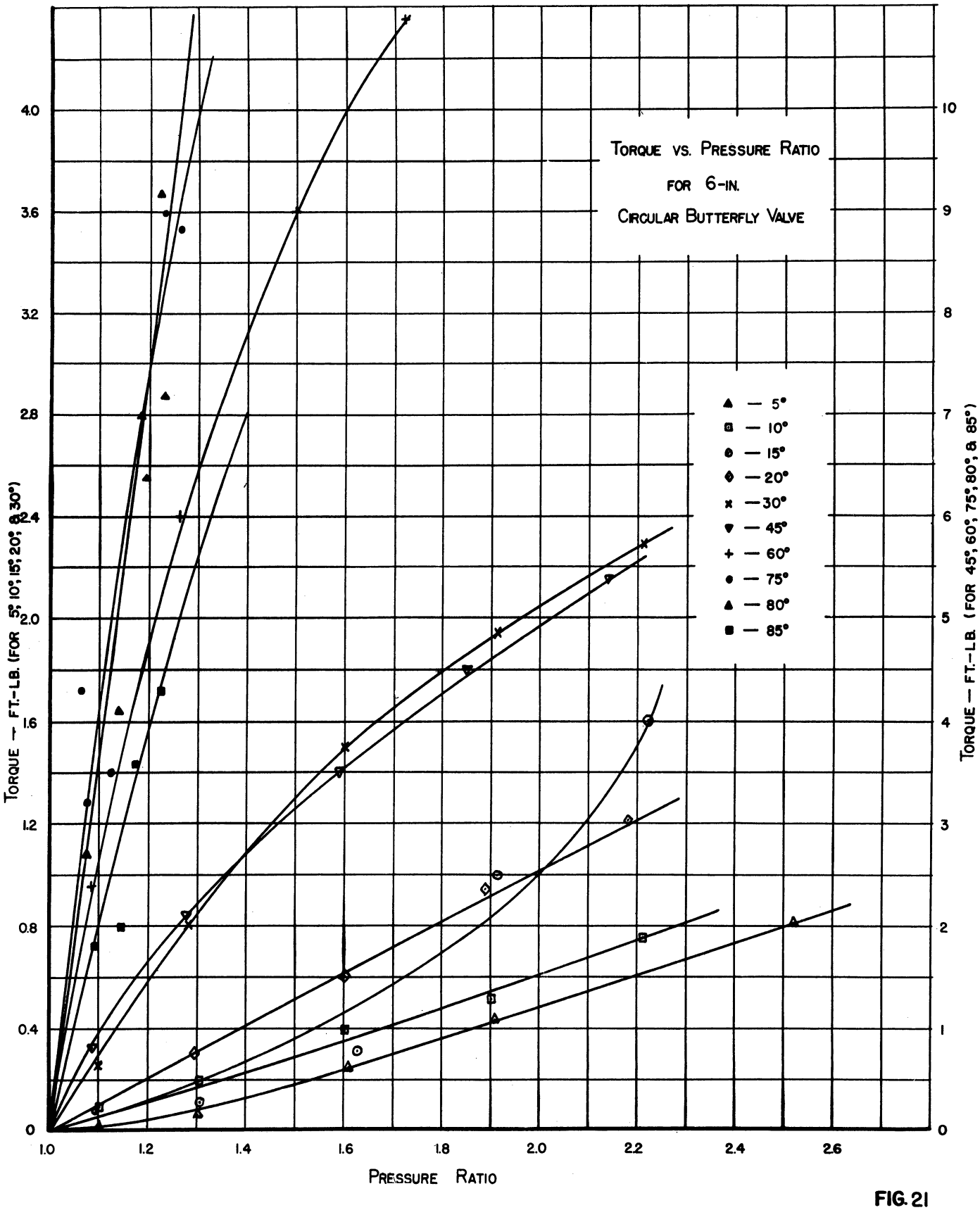
Torque vs. Pressure Ratio
for 6-in.
Circular Butterfly Valve
▲ — 5°
■ — 10°
● — 15°
◆ — 20°
× — 30°
▼ — 45°
+ — 60°
● — 75°
▲ — 80°
■ — 85°
Torque — Ft.-Lb. (for 5°, 10°, 15°, 20°, & 30°)
Torque — Ft.-Lb. (for 45°, 60°, 75°, 80°, & 85°)
Pressure Ratio
0
0.4
0.8
1.2
1.6
2.0
2.4
2.8
3.2
3.6
4.0
1
2
3
4
5
6
7
8
9
10
1.0
1.2
1.4
1.6
1.8
2.0
2.2
2.4
2.6

FIG. 21

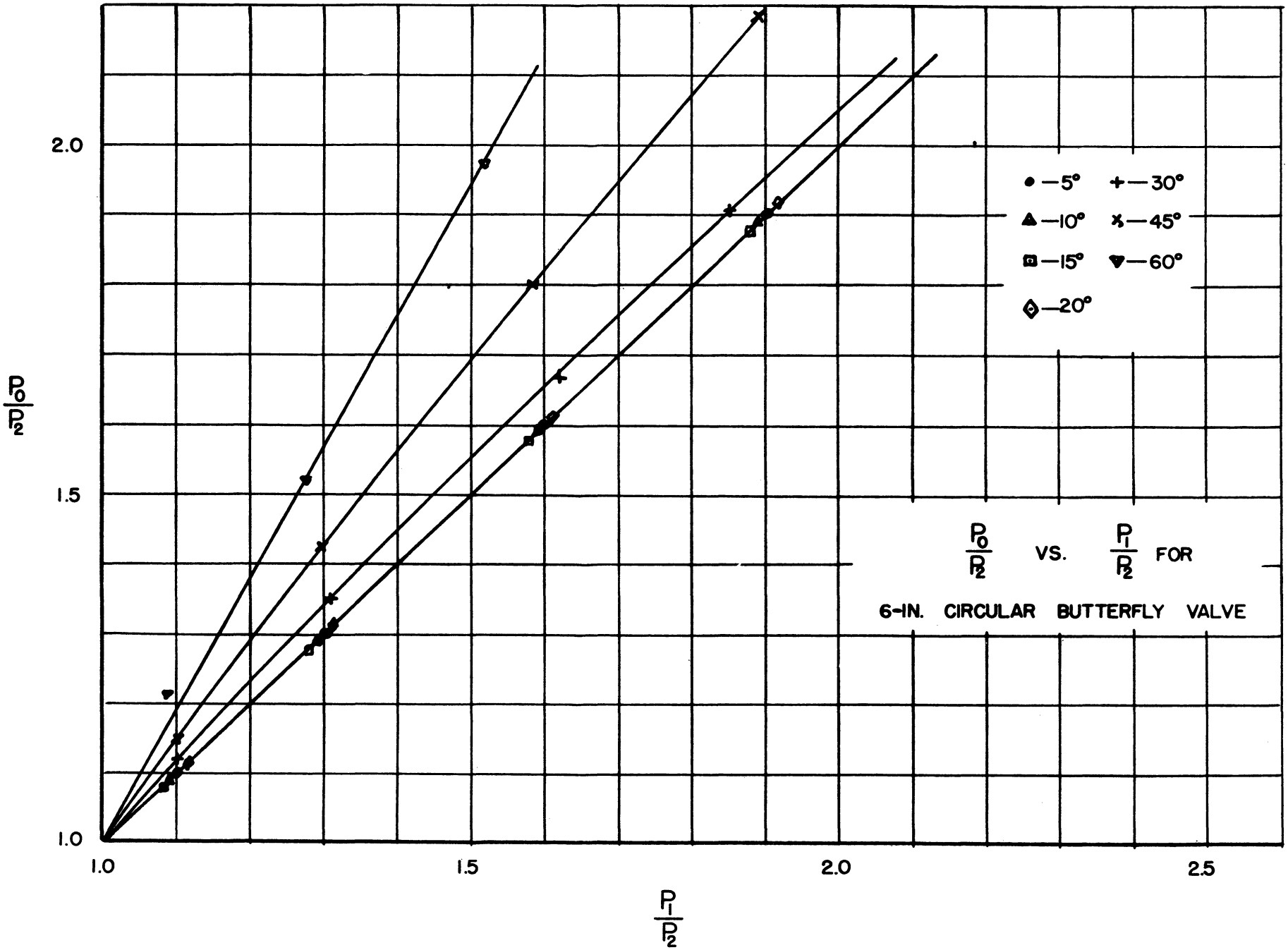
2.0
1.5
1.0
1.0
1.5
2.0
2.5
$\frac{P_0}{P_2}$
$\frac{P_1}{P_2}$
● —5°
+ —30°
▲ —10°
× —45°
■ —15°
▼ —60°
◆ —20°
$\frac{P_0}{P_2}$ VS. $\frac{P_1}{P_2}$ FOR
6-IN. CIRCULAR BUTTERFLY VALVE

FIG. 22

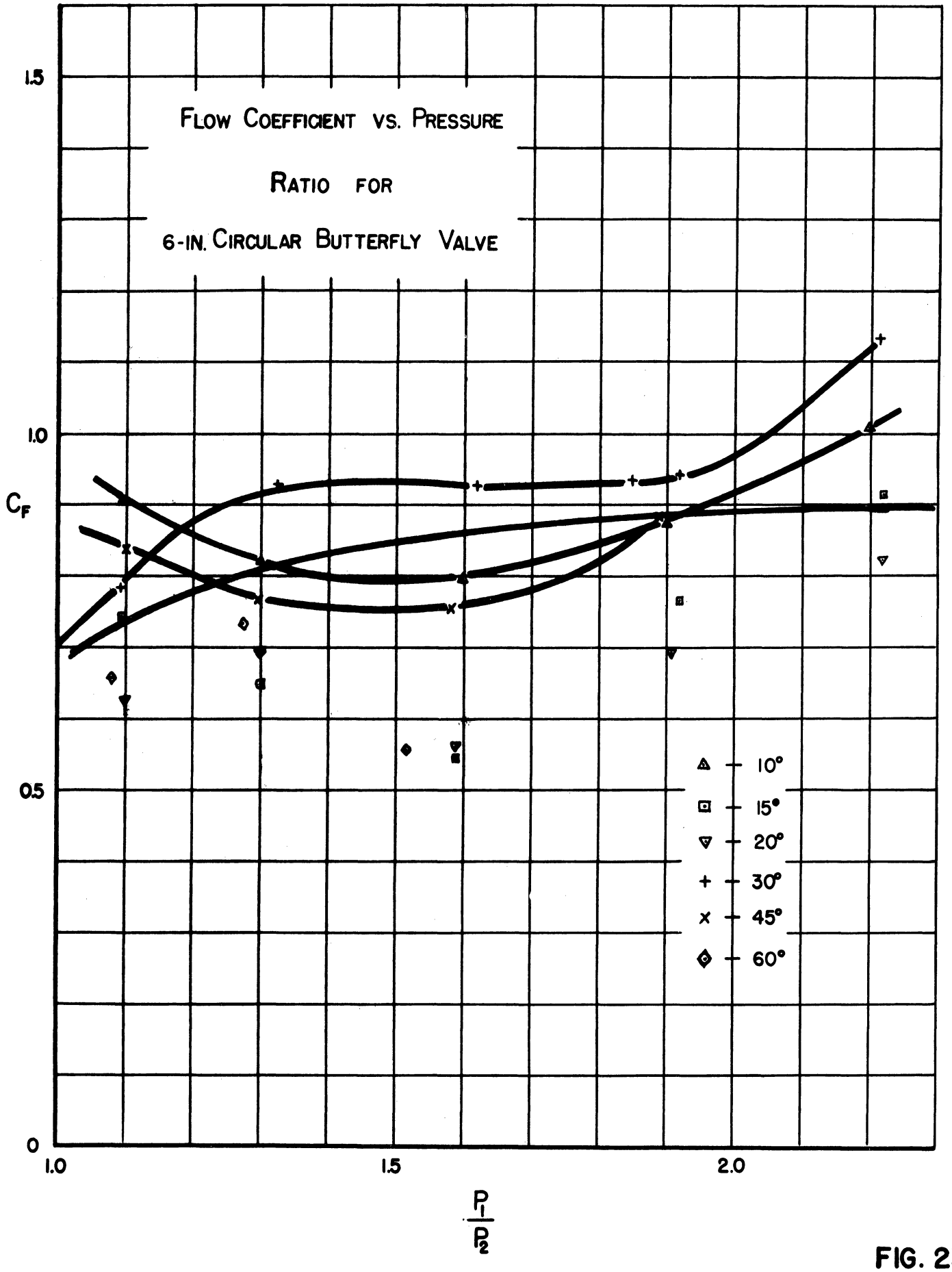
FLOW COEFFICIENT VS. PRESSURE
RATIO FOR
6-IN. CIRCULAR BUTTERFLY VALVE
1.5
1.0
0.5
0
C_F
1.0
1.5
2.0
$\frac{P_1}{P_2}$
10°
15°
20°
30°
45°
60°

FIG. 23

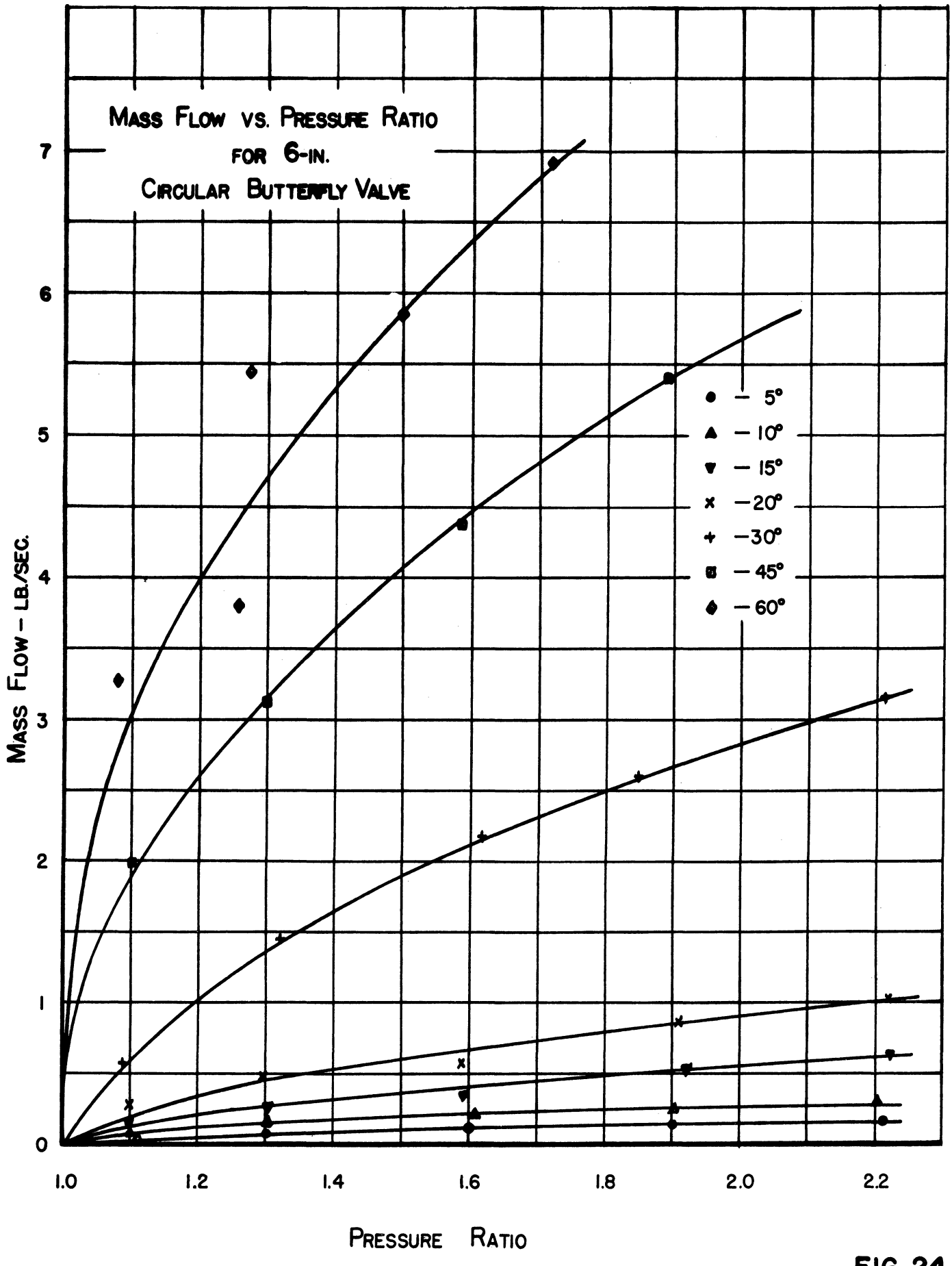
MASS FLOW VS. PRESSURE RATIO
FOR 6-IN.
CIRCULAR BUTTERFLY VALVE
MASS FLOW - LB./SEC.
PRESSURE RATIO
0
1
2
3
4
5
6
7
1.0
1.2
1.4
1.6
1.8
2.0
2.2
5°
10°
15°
20°
30°
45°
60°

FIG. 24

It will be noted that there is a residual torque at all pressure ratios for a valve angle of 0°. This is due to a lack of perfect symmetry in the valve plate construction (Fig. 20).

IV. FLOW AND TORQUE CHARACTERISTICS OF A SEGMENTAL BUTTERFLY VALVE

The tests made on the circular butterfly valve have been repeated for the segmental valve (Figs. 25-28). In general, the comments made about the circular valve also apply to the segmental valve. The torque data have been extended to cover larger angles and pressure ratios than for the circular valve, because the segmental valve is smaller in area and it was therefore possible to develop higher pressure ratios across it (Figs. 30, 31, and 32).

A small amount of residual torque at zero valve angle that results from a lack of symmetry in the valve plate has been faired out in Fig. 31.

For measuring the plate pressures, three taps on the plate were used (Fig. 28). There are four possible arrangements for the three taps, depending on the manner of turning the valve plate and the direction of air flow. These four arrangements or configurations are shown as A and B (Fig. 13) and C and D (Fig. 29).

The plate pressures of the segmental valve have been taken from the tap configuration B used in the circular valve and from tap configuration C. Time limitations did not permit plate pressure measurements at all possible configurations, and it was felt that configurations B and C were the most significant for the segmental valve.

The ratios of the plate tap pressures (P_{v1}, P_{v2}, P_{v3}) to the downstream valve static pressure are plotted against the overall valve static pressure ratio in Figs. 34-39. The downstream static pressure is one atmosphere.

It will be noted that there is considerable difference in the configuration B plate pressure curves for the circular and the segmental valves. No explanation is offered for this, but the results show that it would be unwise to make generalizations on the plate pressures for other types of valves.

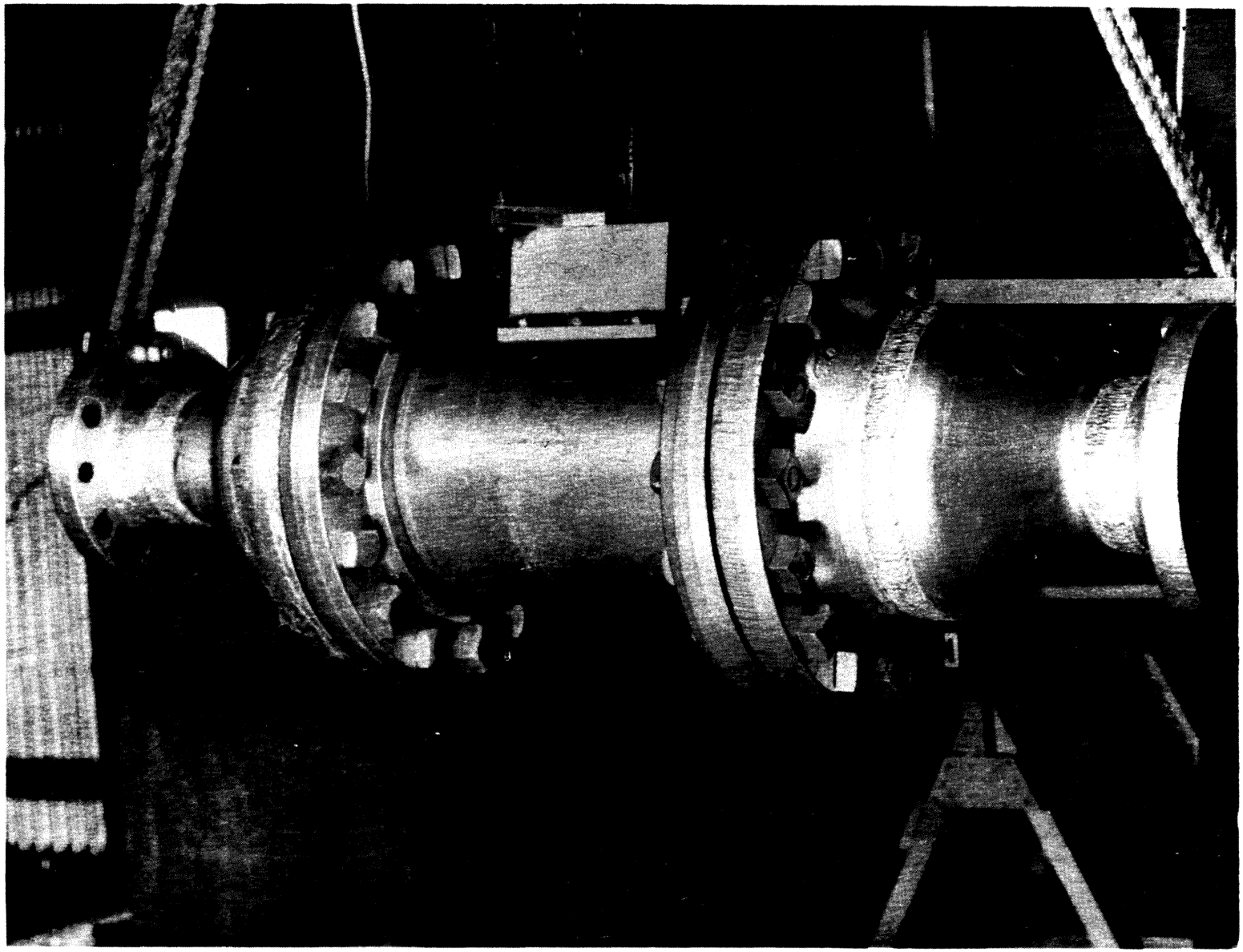

Fig. 25 Photograph of Assembled Segmental Butterfly Valve

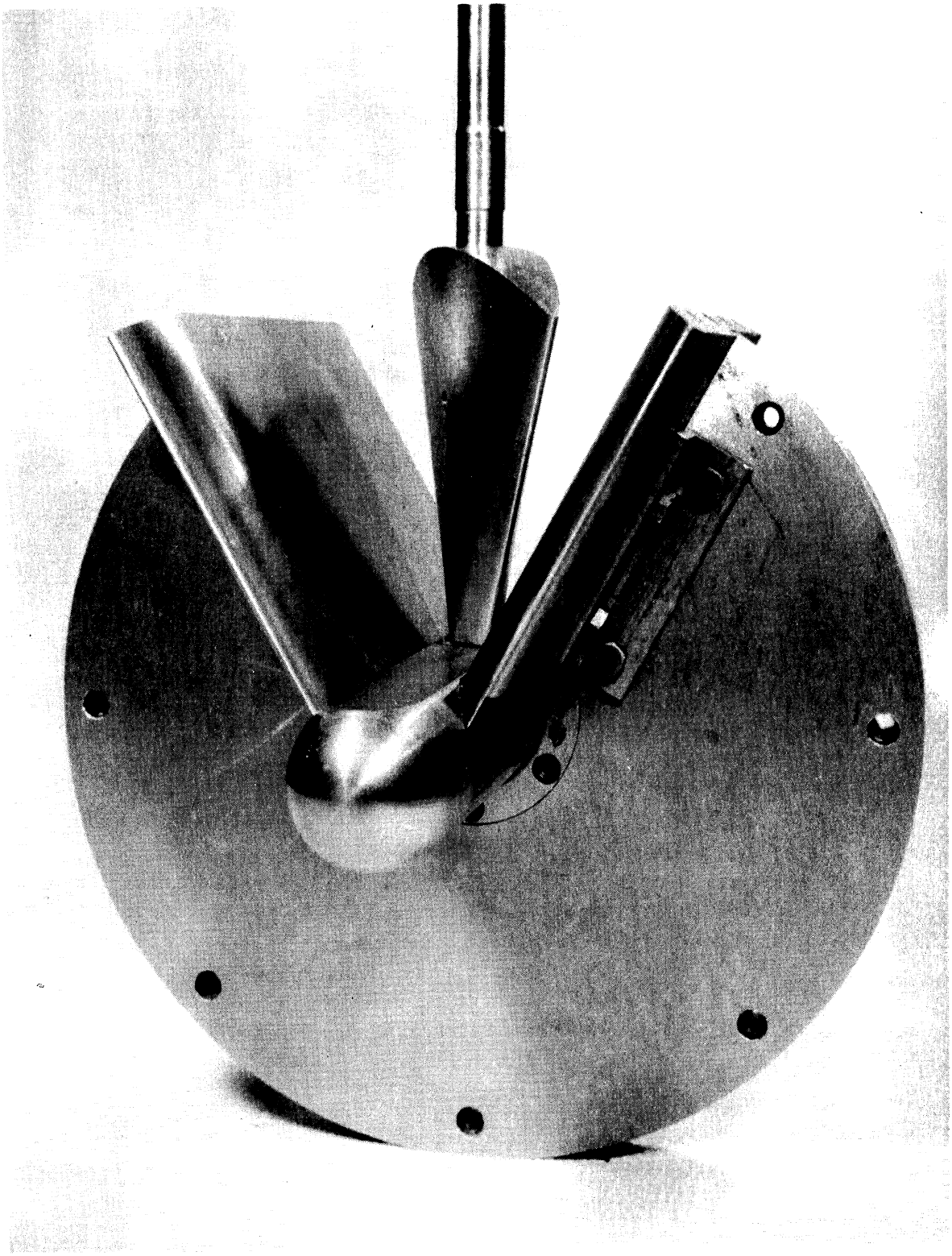

Fig. 26 Phòtograph of Components of
Disassembled Segmental Butterfly Valve

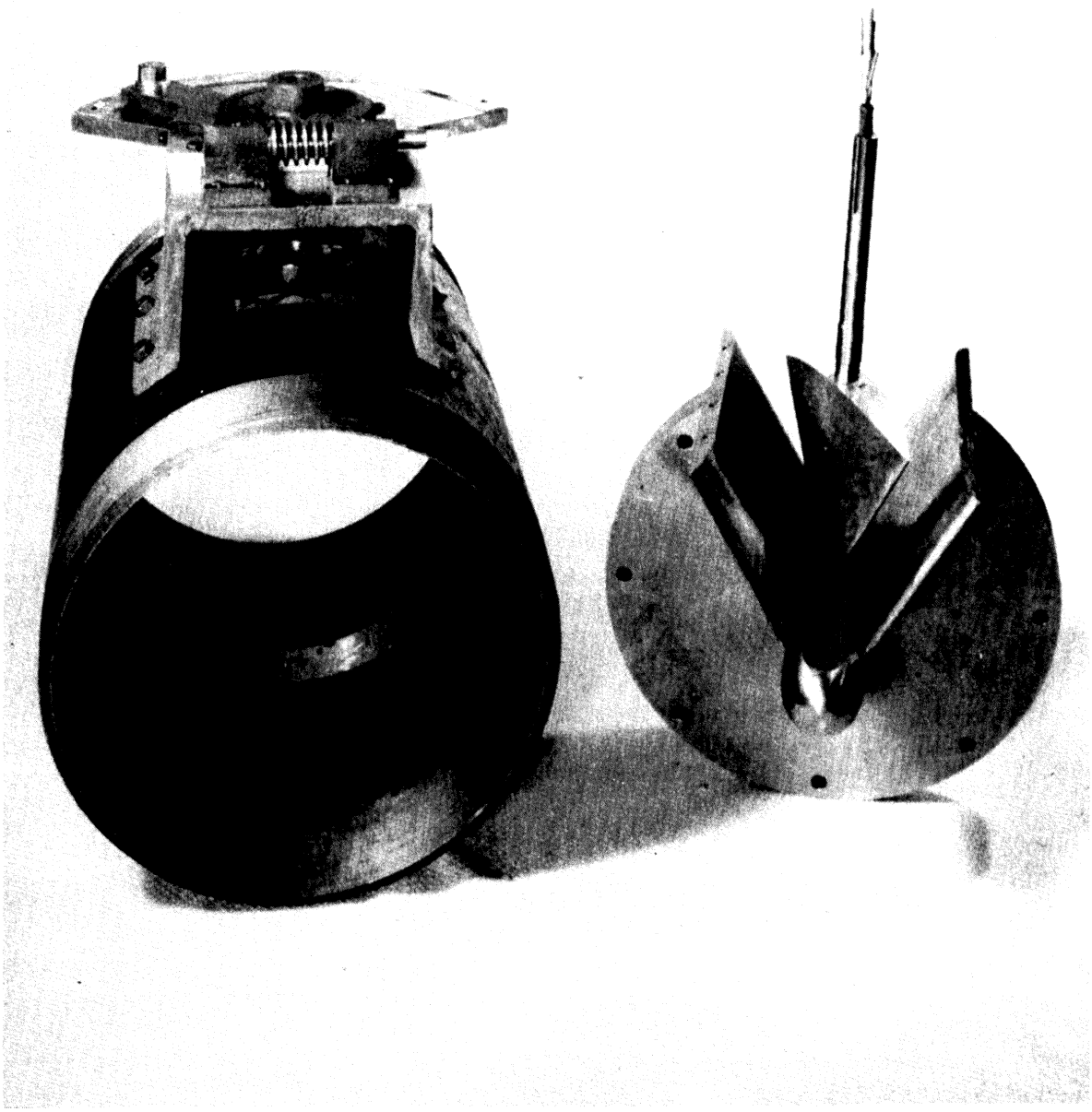

Fig. 27 Photograph of Components of
Disassembled Segmental Butterfly Valve

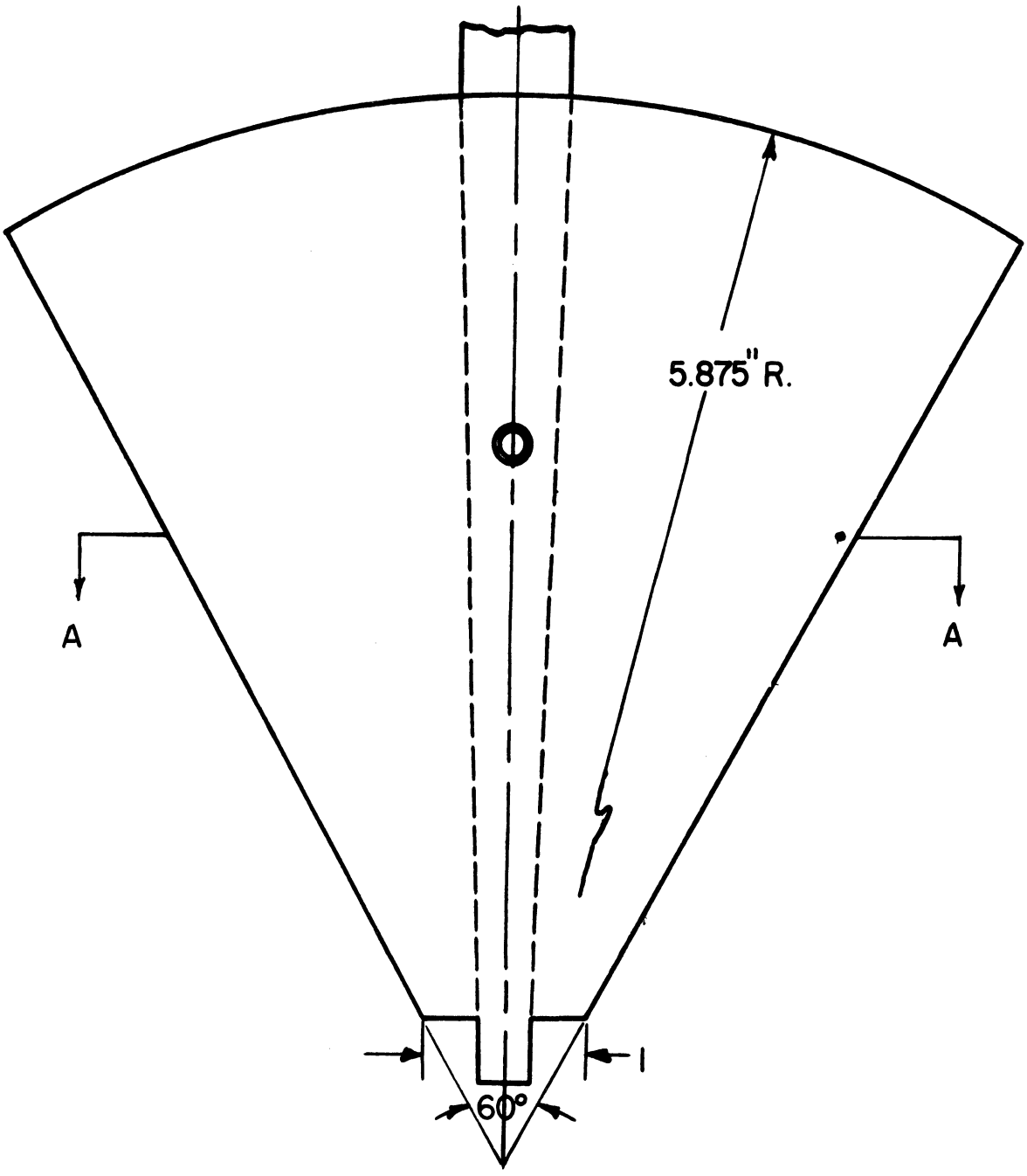

PRESSURE TAP LOCATIONS

ON SEGMENTAL VALVE

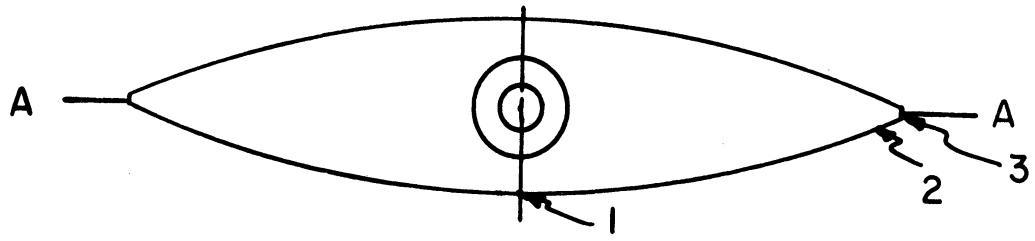

FIG. 28

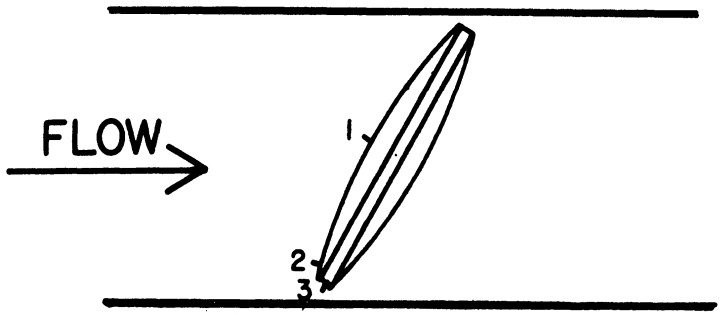

CONFIGURATION - "C"

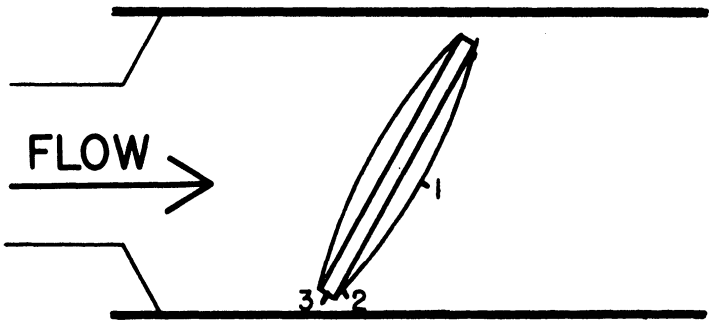

CONFIGURATION "D"

LOCATION OF PRESSURE TAPS ON VALVE PLATE

AWS

FIG. 29

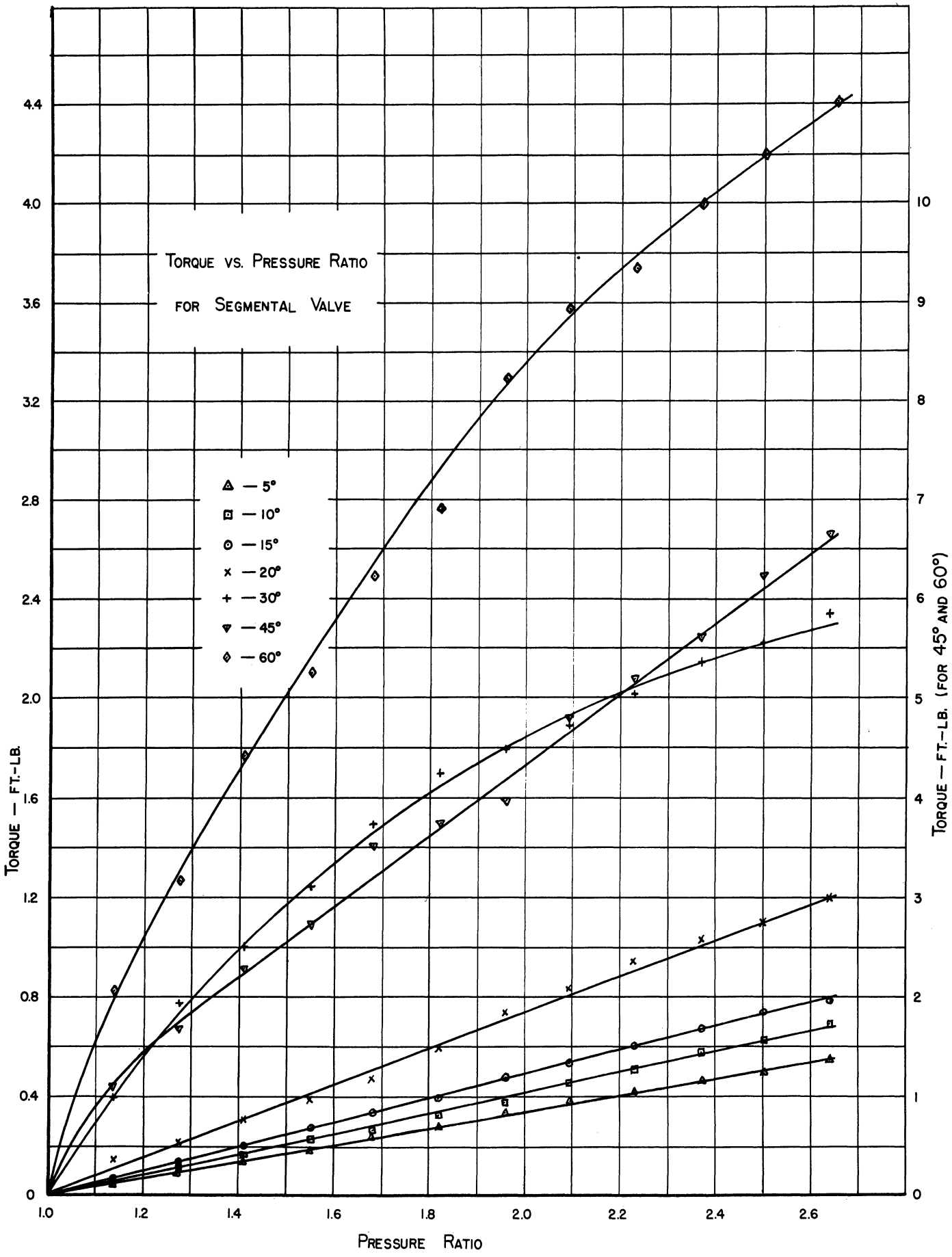
TORQUE VS. PRESSURE RATIO
FOR SEGMENTAL VALVE
— 5°
— 10°
— 15°
— 20°
— 30°
— 45°
— 60°
TORQUE — FT.-LB.
TORQUE — FT.-LB. (FOR 45° AND 60°)
PRESSURE RATIO
0
0.4
0.8
1.2
1.6
2.0
2.4
2.8
3.2
3.6
4.0
4.4
1
2
3
4
5
6
7
8
9
10
1.0
1.2
1.4
1.6
1.8
2.0
2.2
2.4
2.6

FIG. 30

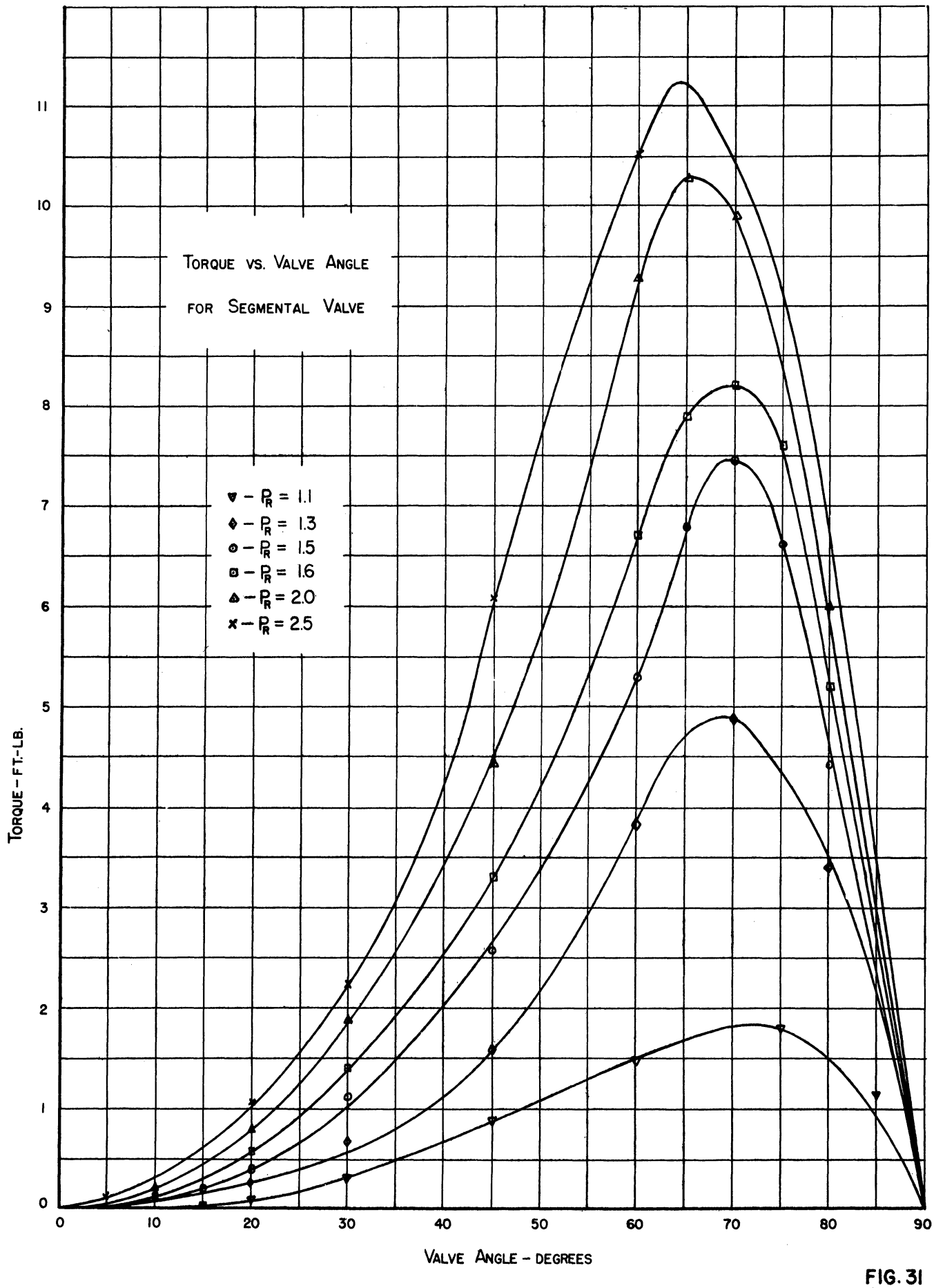
Torque vs. Valve Angle
for Segmental Valve
▼ – P_R = 1.1
♦ – P_R = 1.3
⊙ – P_R = 1.5
□ – P_R = 1.6
△ – P_R = 2.0
× – P_R = 2.5
Torque - Ft.-Lb.
0
1
2
3
4
5
6
7
8
9
10
11
0
10
20
30
40
50
60
70
80
90
Valve Angle - Degrees

FIG. 31

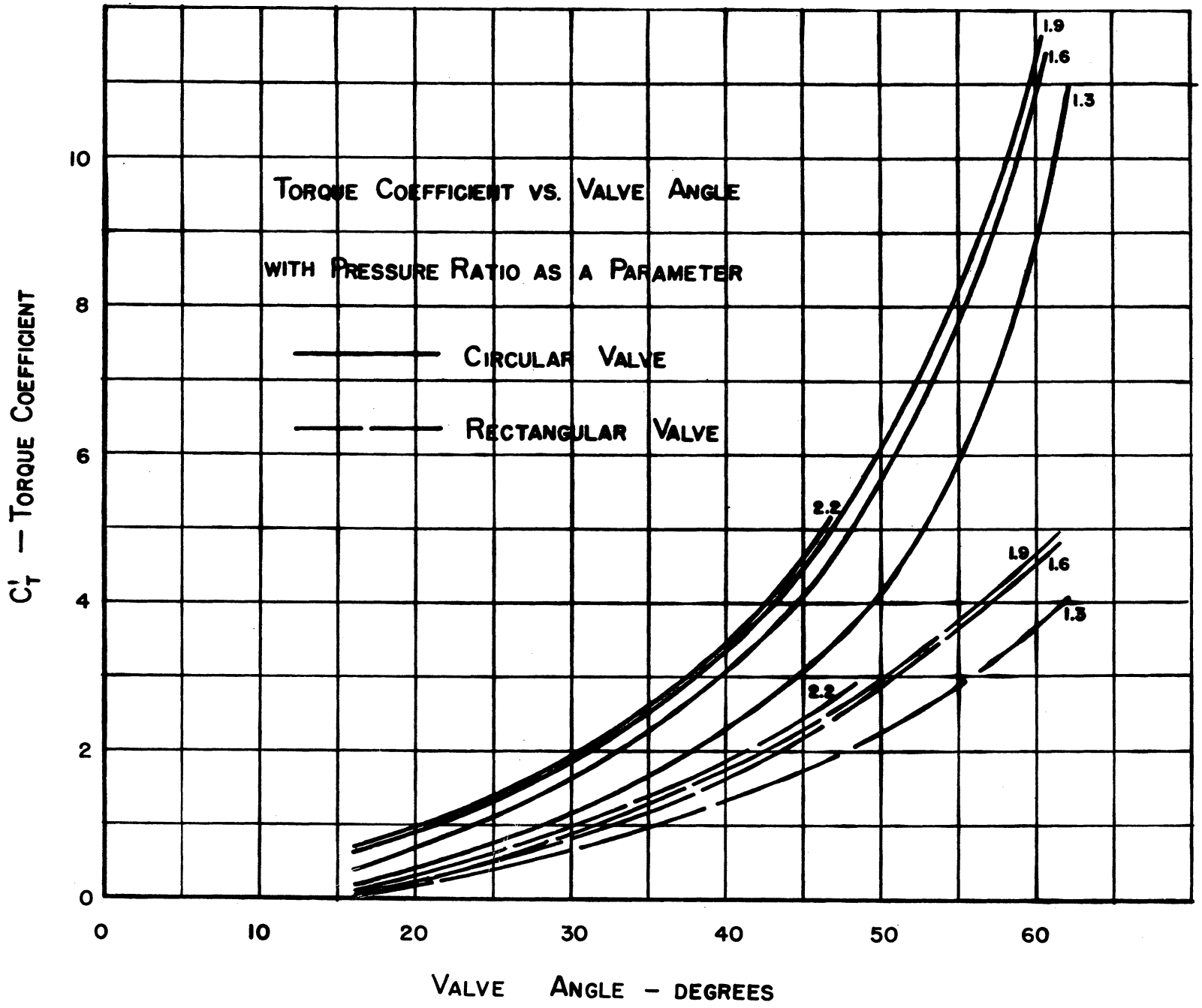
TORQUE COEFFICIENT VS. VALVE ANGLE
WITH PRESSURE RATIO AS A PARAMETER
CIRCULAR VALVE
RECTANGULAR VALVE
1.9
1.6
1.3
2.2
1.9
1.6
1.3
2.2
C_T' — TORQUE COEFFICIENT
0
2
4
6
8
10
0
10
20
30
40
50
60
VALVE ANGLE — DEGREES

FIG. 32a

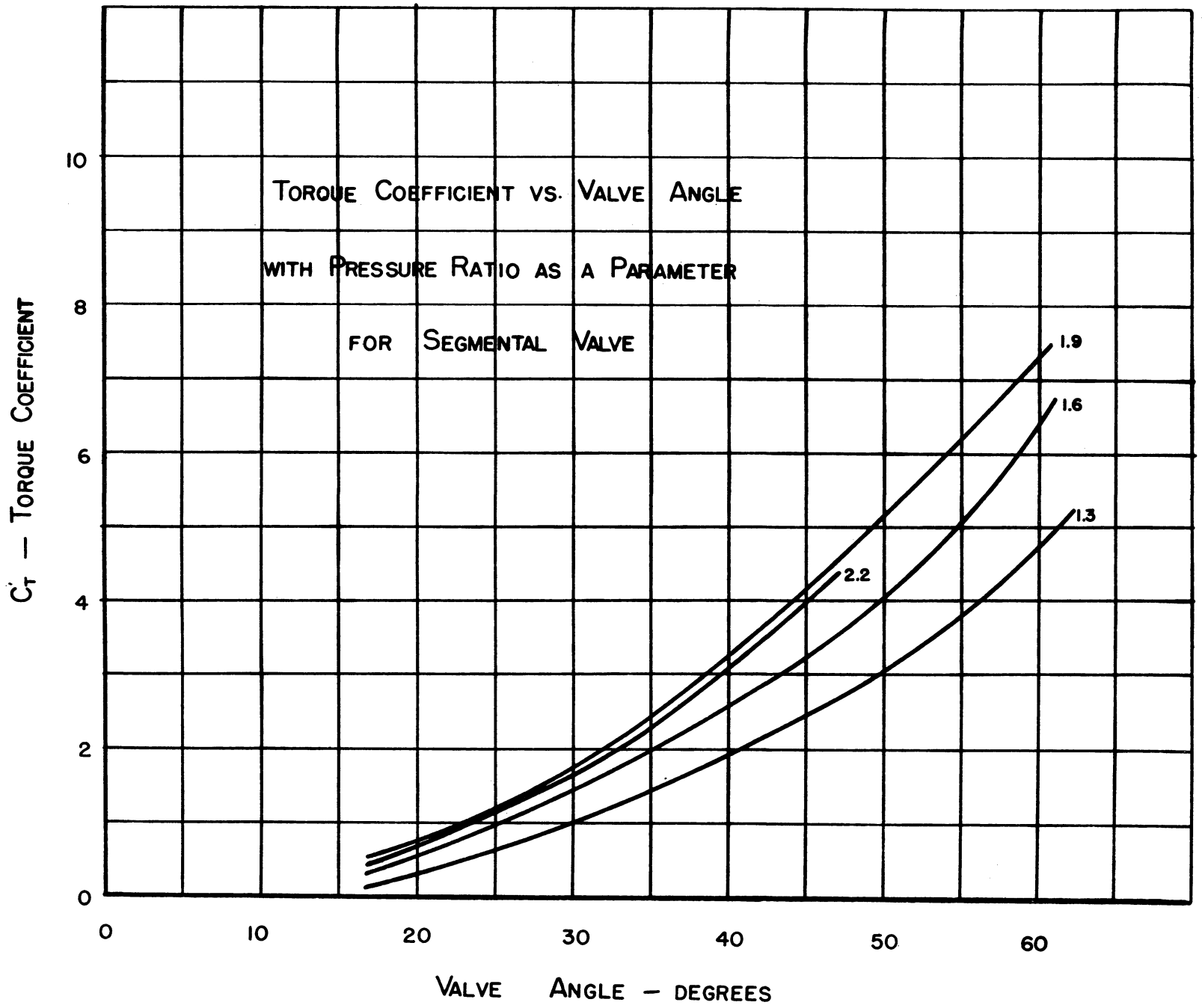
TORQUE COEFFICIENT VS. VALVE ANGLE
WITH PRESSURE RATIO AS A PARAMETER
FOR SEGMENTAL VALVE
1.9
1.6
1.3
2.2
C_T — TORQUE COEFFICIENT
0
2
4
6
8
10
0
10
20
30
40
50
60
VALVE ANGLE — DEGREES

FIG. 32b

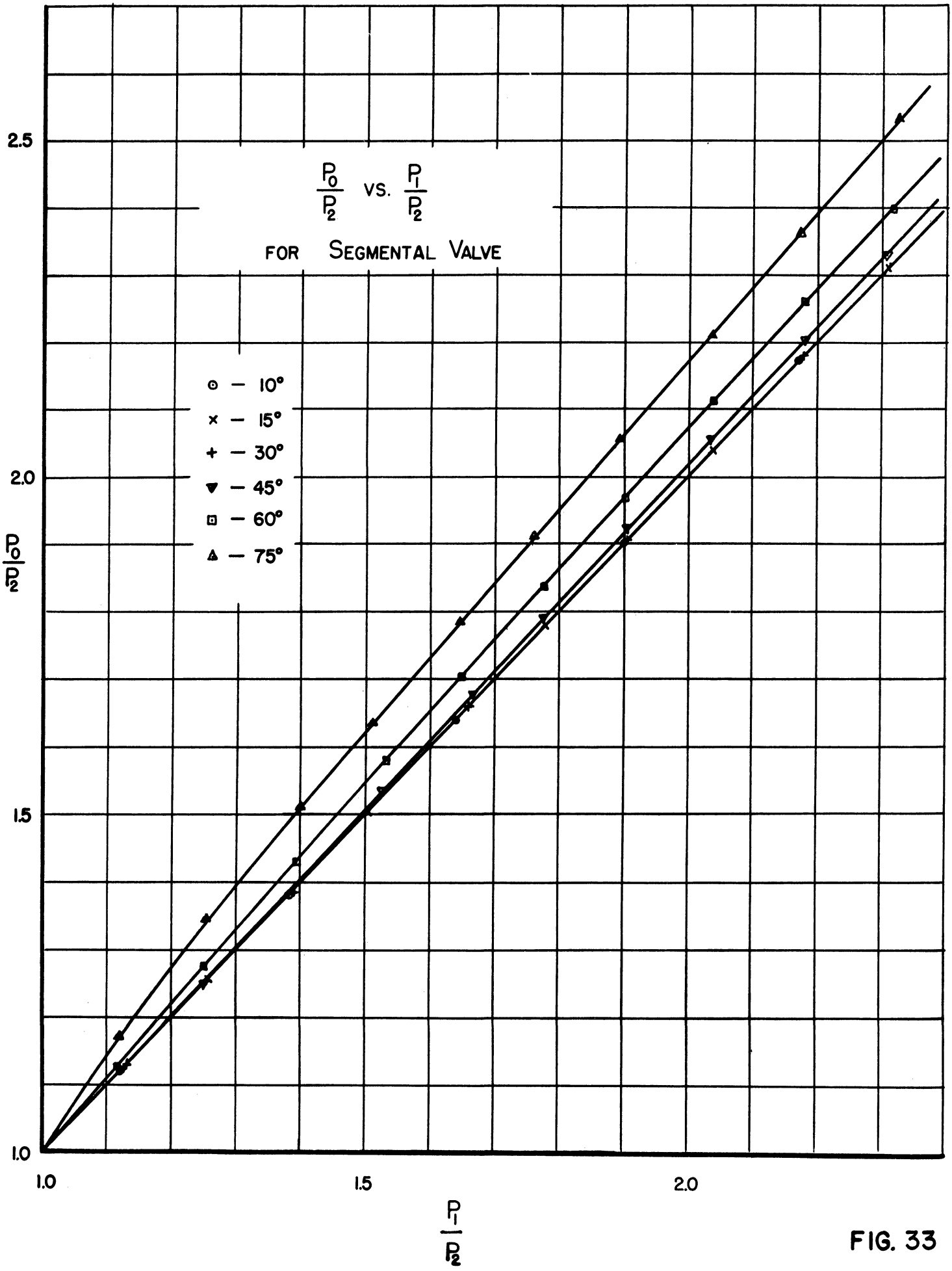
$\frac{P_0}{P_2}$ vs. $\frac{P_1}{P_2}$
FOR SEGMENTAL VALVE
⊙ — 10°
× — 15°
+ — 30°
▼ — 45°
⊡ — 60°
▲ — 75°
2.5
2.0
1.5
1.0
$\frac{P_0}{P_2}$
1.0
1.5
2.0
$\frac{P_1}{P_2}$

FIG. 33

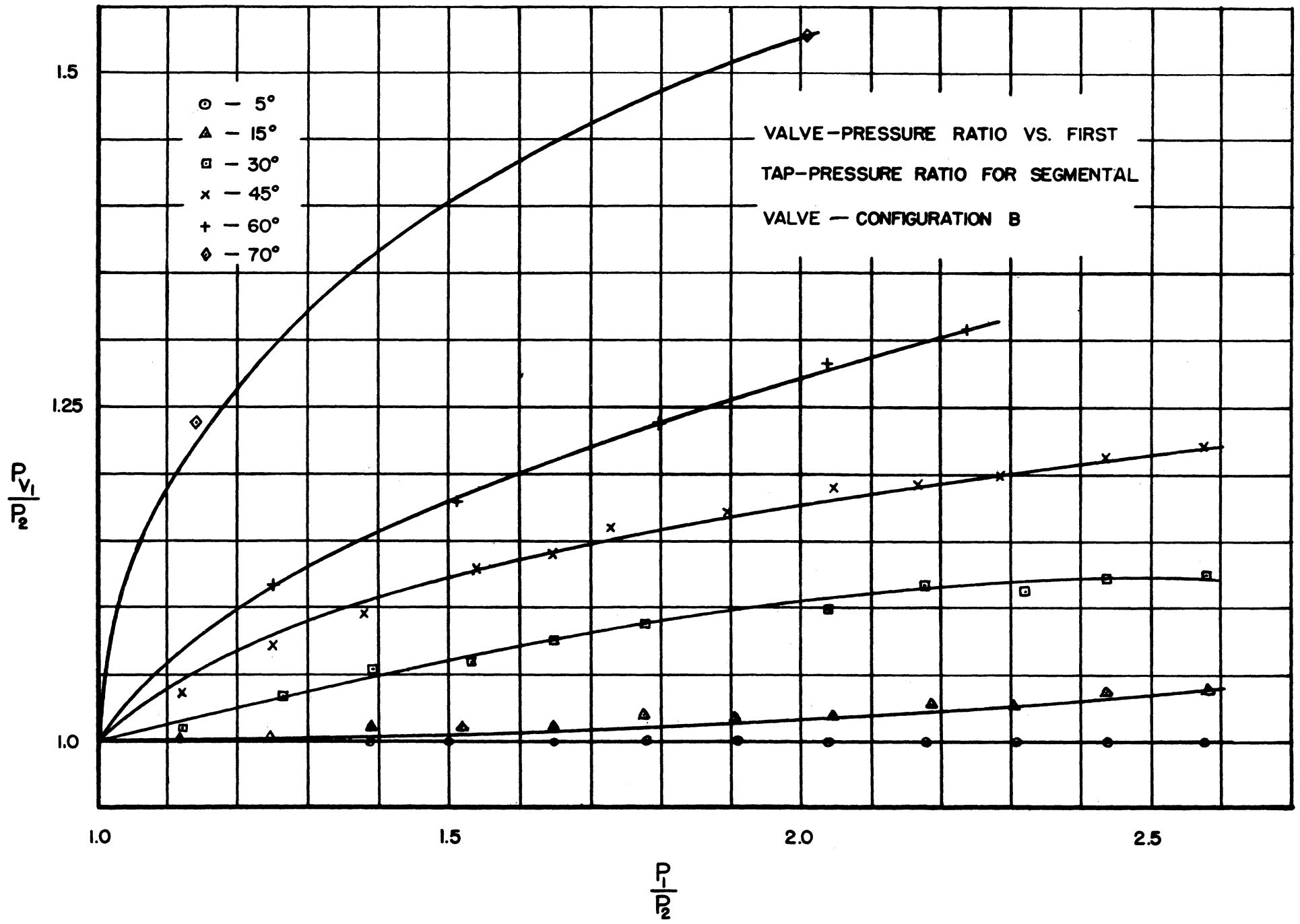
VALVE—PRESSURE RATIO VS. FIRST TAP—PRESSURE RATIO FOR SEGMENTAL VALVE — CONFIGURATION B
⊙ — 5°
△ — 15°
⊡ — 30°
× — 45°
+ — 60°
◇ — 70°
1.5
1.25
1.0
$\frac{P_{V1}}{P_2}$
1.0
1.5
2.0
2.5
$\frac{P_1}{P_2}$

FIG. 34

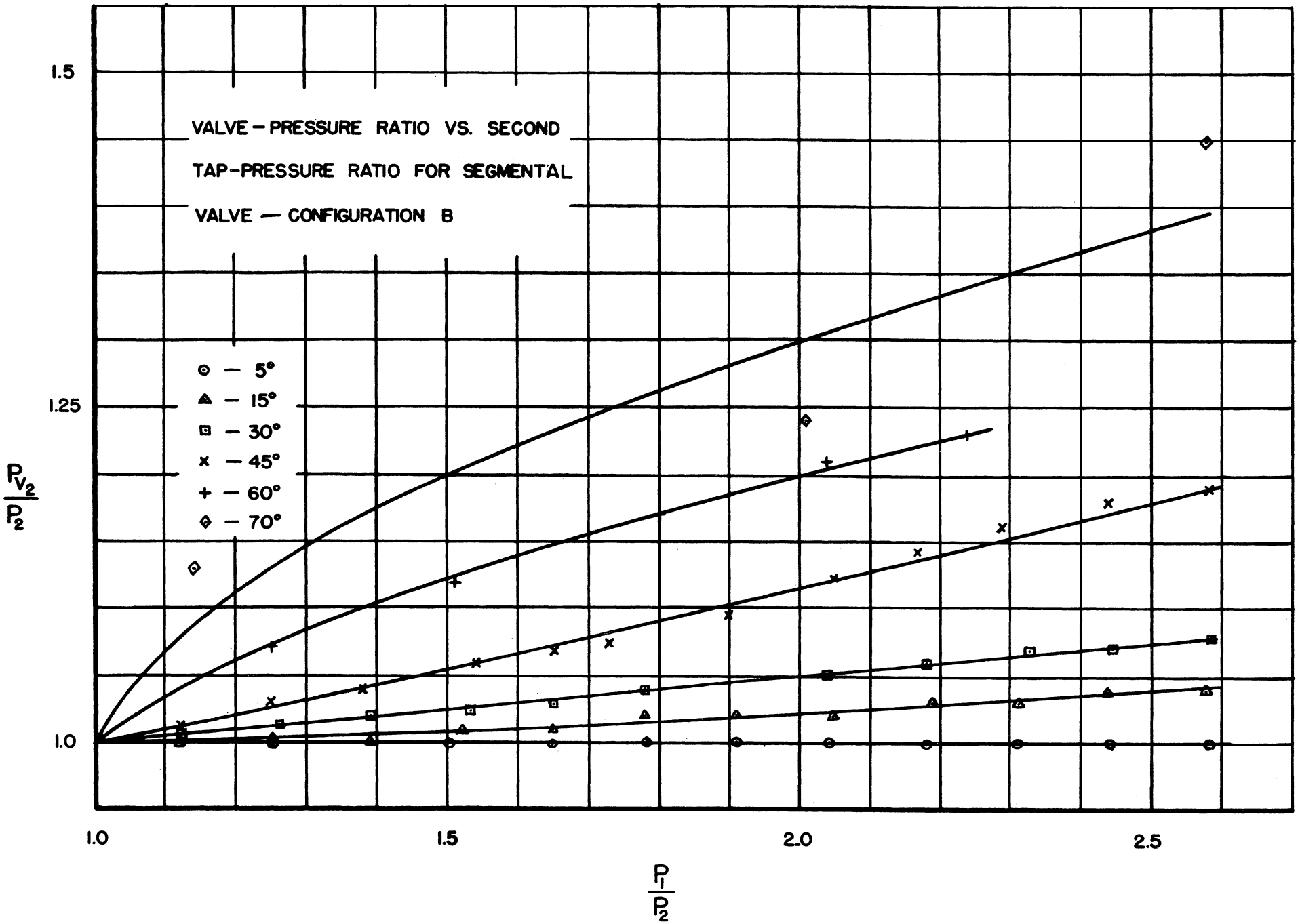
VALVE – PRESSURE RATIO VS. SECOND TAP-PRESSURE RATIO FOR SEGMENTAL VALVE — CONFIGURATION B
⊙ – 5°
▲ – 15°
⊡ – 30°
× – 45°
+ – 60°
◇ – 70°
1.5
1.25
1.0
$\frac{P_{V_2}}{P_2}$
1.0
1.5
2.0
2.5
$\frac{P_1}{P_2}$

FIG. 35

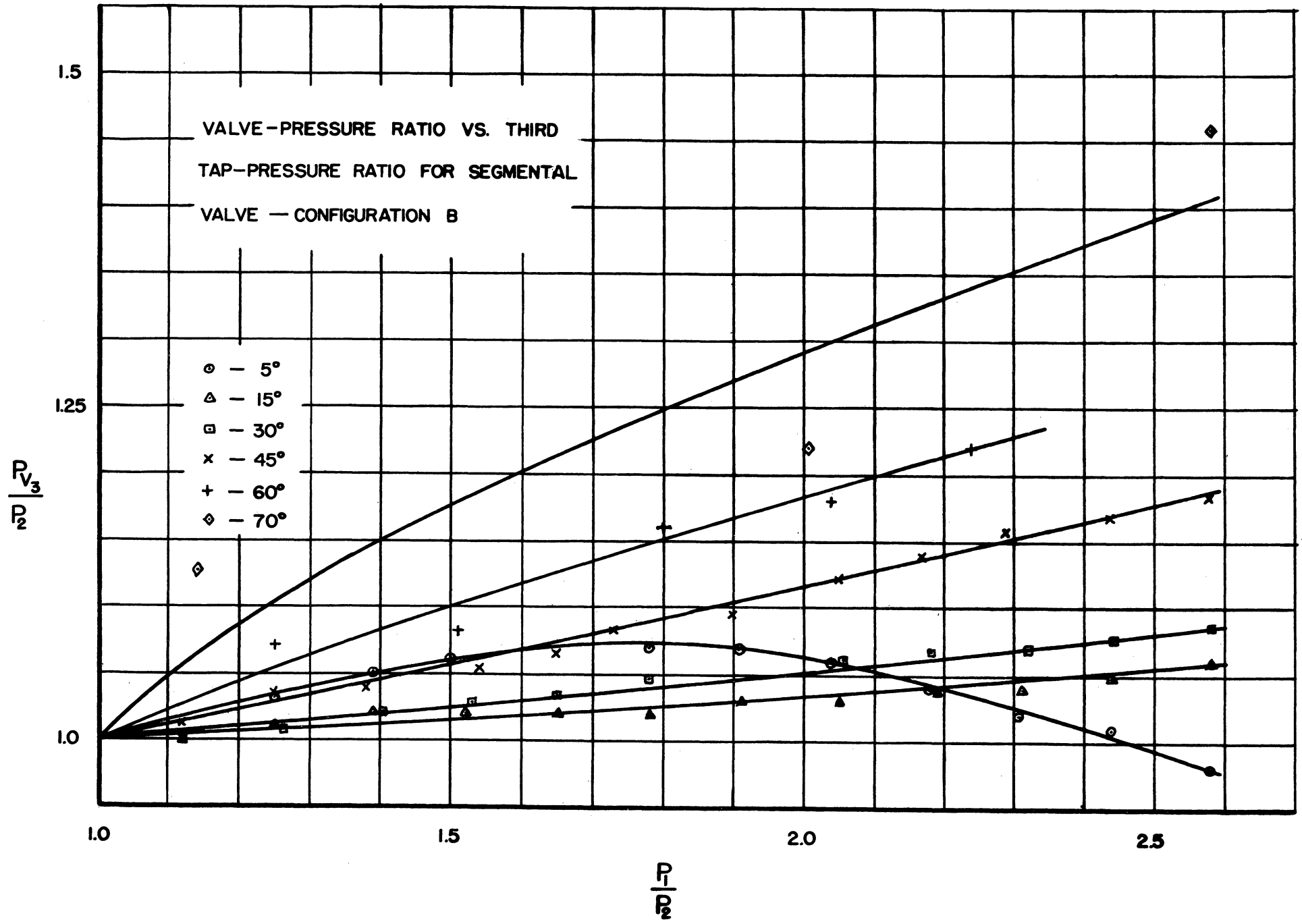
VALVE-PRESSURE RATIO VS. THIRD
TAP-PRESSURE RATIO FOR SEGMENTAL
VALVE — CONFIGURATION B
⊙ — 5°
△ — 15°
□ — 30°
× — 45°
+ — 60°
◇ — 70°
1.5
1.25
1.0
$\frac{P_{V_3}}{P_2}$
1.0
1.5
2.0
2.5
$\frac{P_1}{P_2}$

FIG. 36

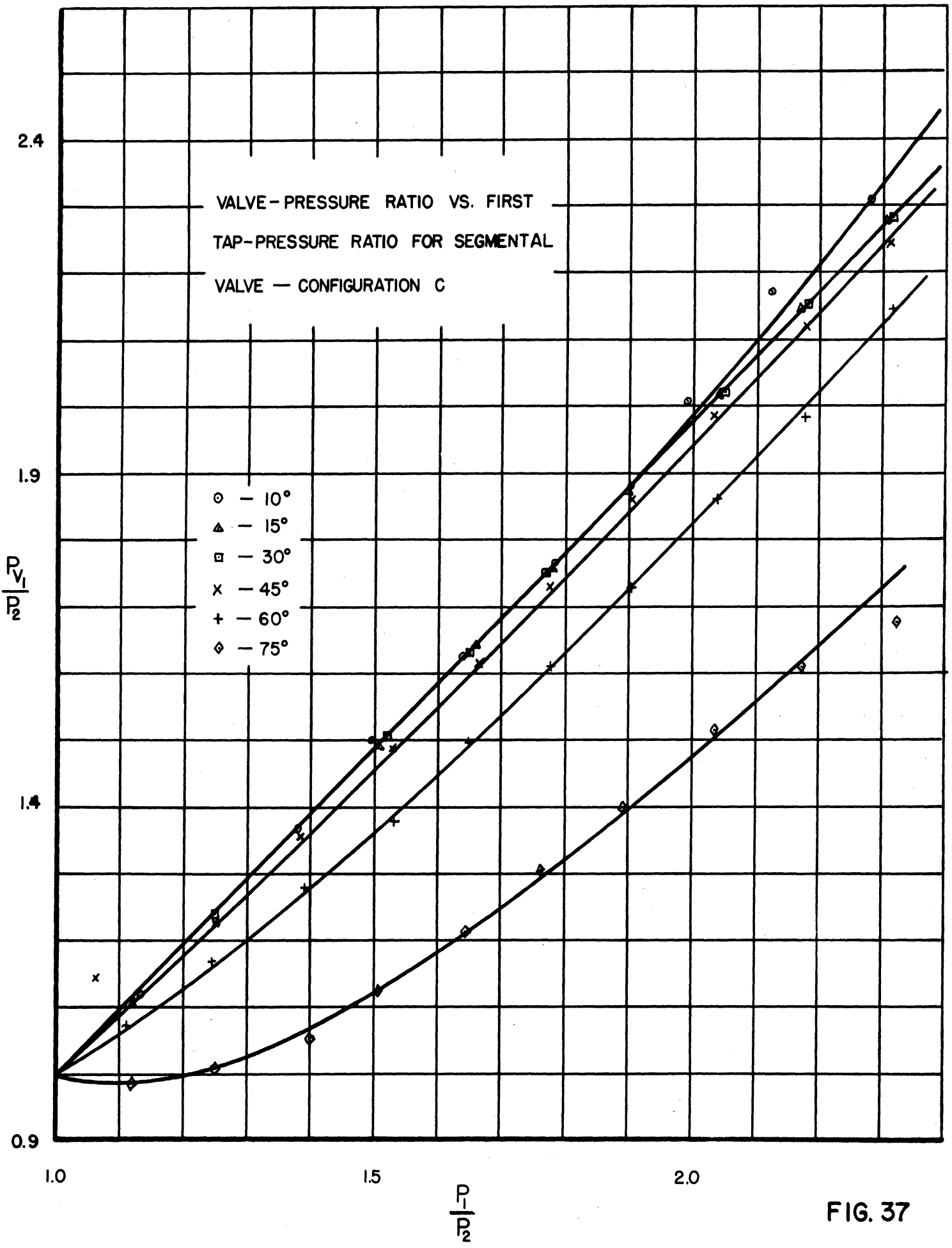
VALVE - PRESSURE RATIO VS. FIRST
TAP - PRESSURE RATIO FOR SEGMENTAL
VALVE — CONFIGURATION C
⊙ — 10°
△ — 15°
⊡ — 30°
× — 45°
+ — 60°
◇ — 75°
2.4
1.9
1.4
0.9
$\frac{P_{V_1}}{P_2}$
1.0
1.5
2.0
$\frac{P_1}{P_2}$

FIG. 37

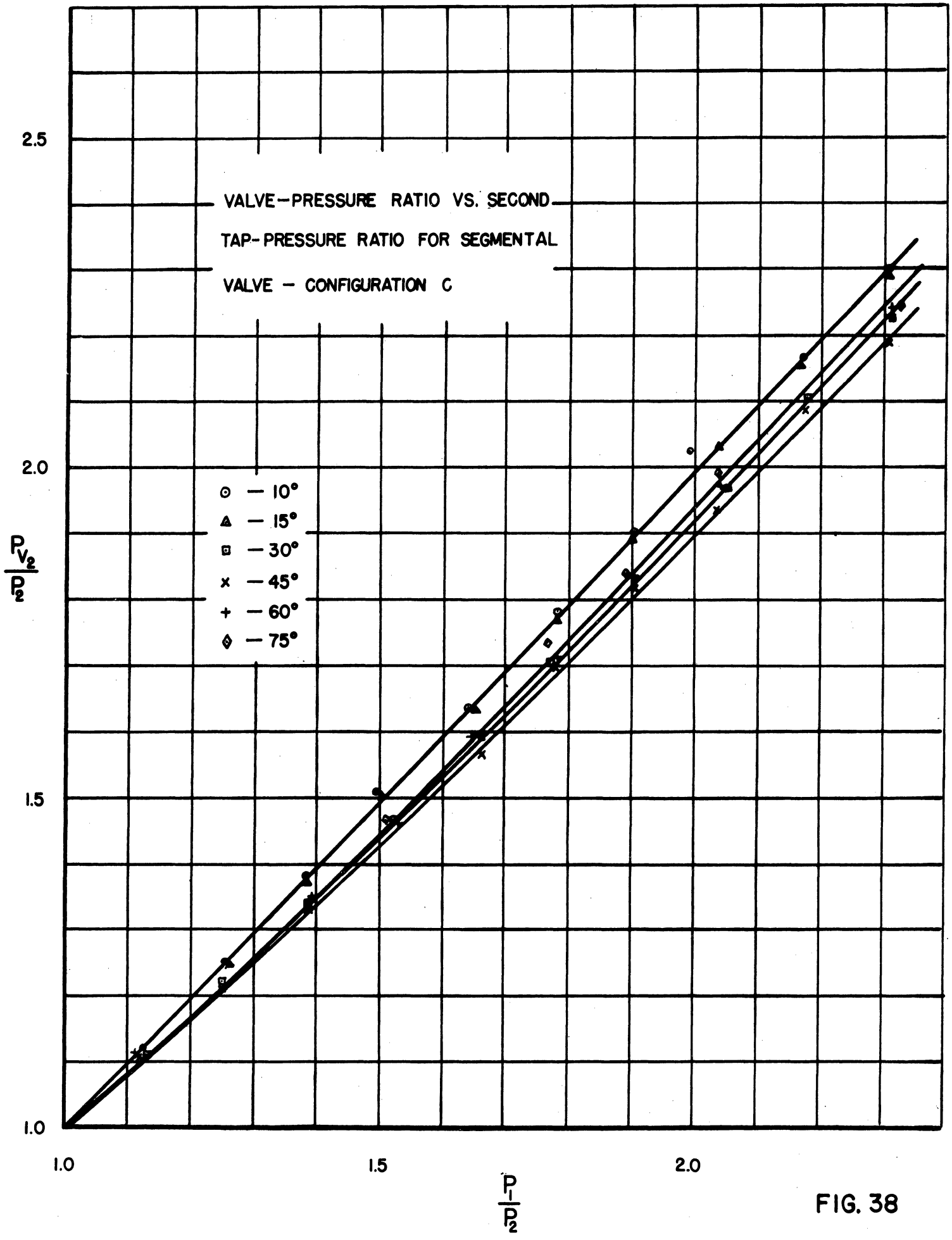
VALVE–PRESSURE RATIO VS. SECOND TAP-PRESSURE RATIO FOR SEGMENTAL VALVE – CONFIGURATION C
⊙ — 10°
▲ — 15°
⊡ — 30°
× — 45°
+ — 60°
◈ — 75°
2.5
2.0
1.5
1.0
$\frac{P_{V_2}}{P_2}$
1.0
1.5
2.0
$\frac{P_1}{P_2}$

FIG. 38

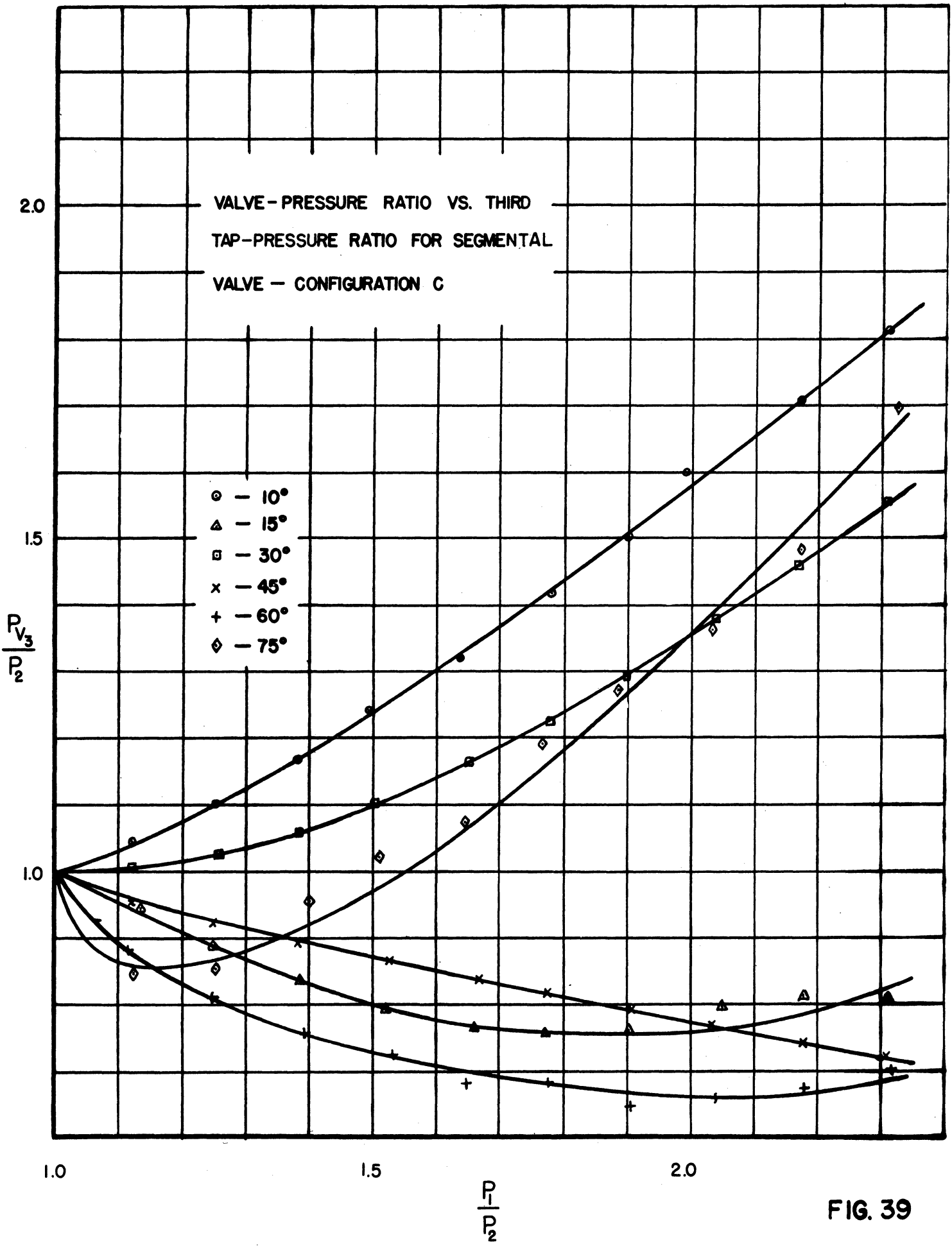
VALVE - PRESSURE RATIO VS. THIRD
TAP-PRESSURE RATIO FOR SEGMENTAL
VALVE — CONFIGURATION C
⊙ — 10°
△ — 15°
⊡ — 30°
× — 45°
+ — 60°
◇ — 75°
2.0
1.5
1.0
$\frac{P_{V_3}}{P_2}$
1.0
1.5
2.0
$\frac{P_1}{P_2}$

FIG. 39

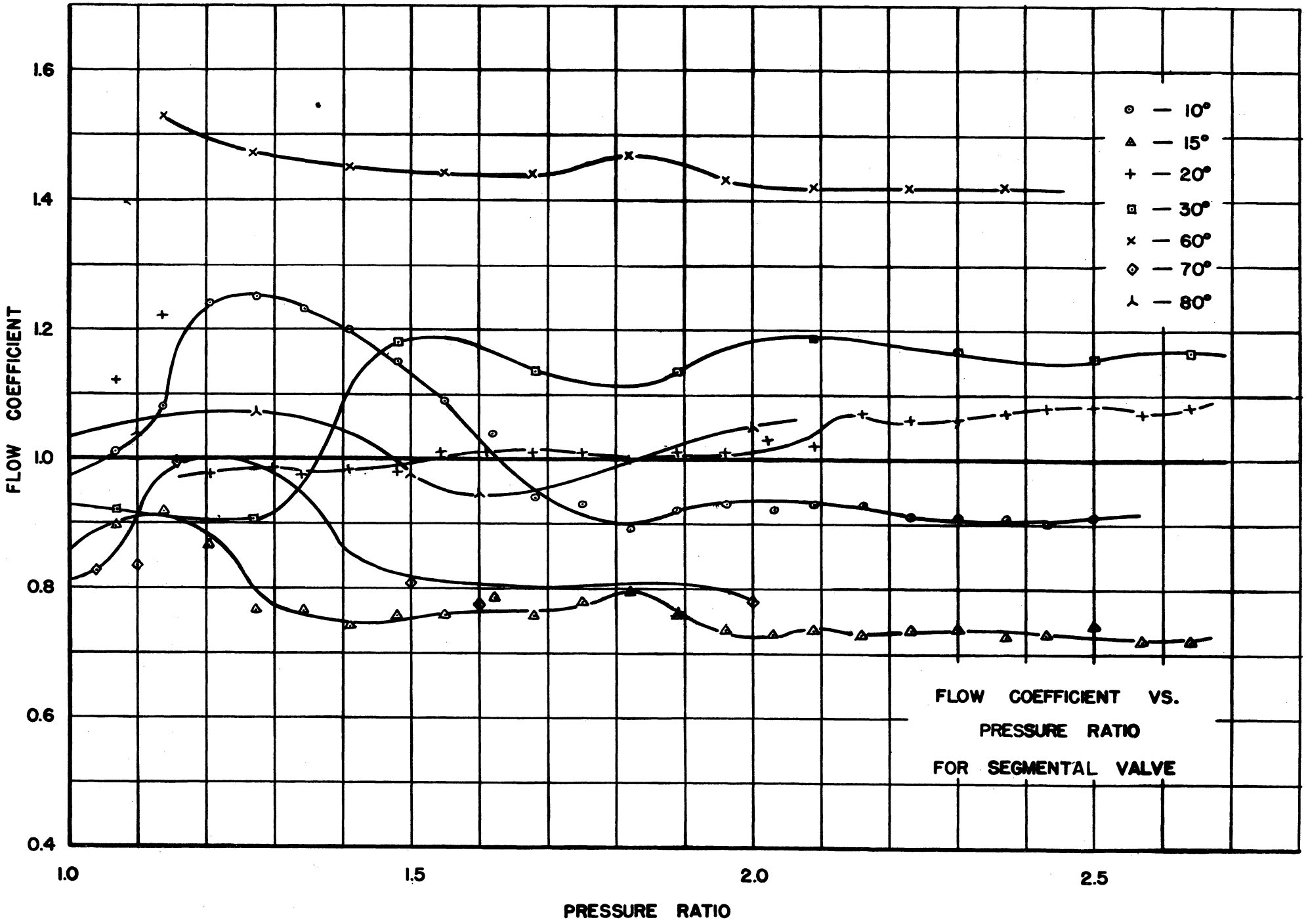
FLOW COEFFICIENT
1.6
1.4
1.2
1.0
0.8
0.6
0.4
1.0
1.5
2.0
2.5
PRESSURE RATIO
10°
15°
20°
30°
60°
70°
80°
FLOW COEFFICIENT VS.
PRESSURE RATIO
FOR SEGMENTAL VALVE

FIG. 40

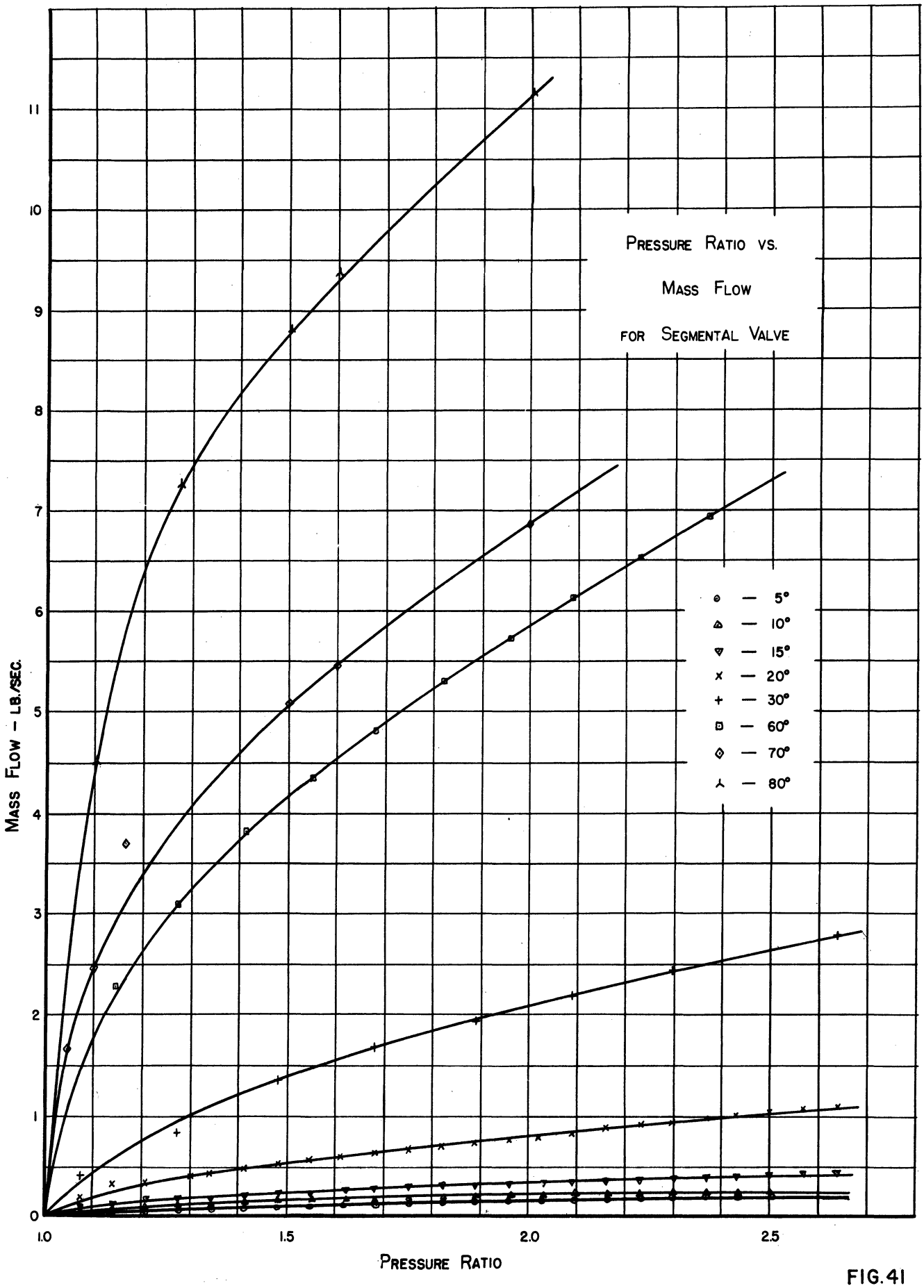
PRESSURE RATIO VS.
MASS FLOW
FOR SEGMENTAL VALVE
⊙ — 5°
△ — 10°
▽ — 15°
× — 20°
+ — 30°
□ — 60°
◇ — 70°
⅄ — 80°
MASS FLOW - LB./SEC.
0
1
2
3
4
5
6
7
8
9
10
11
1.0
1.5
2.0
2.5
PRESSURE RATIO

FIG. 41

APPENDICES

APPENDIX A

TEMPERATURE CORRECTION FOR A THERMOCOUPLE

The determination of the temperature lag of the thermocouple elements inside the air tank is complicated by several factors. The elements may be considered to be cooled by natural convection, but the air convection at the thermocouple is modified by the convection currents set up in the tank due to wall heating. Furthermore, there are forced air currents due to the removal of air from the tank. Radiation effects further complicated the situation, and in addition there is the effect of thermal conductivity of the attached leads.

Considering all this, it appears that an experimental determination of the temperature lag is the most realistic approach. Ordinarily, this could be accomplished conveniently only in the atmosphere; it is doubtful that this method would give reliable results when extended to the conditions inside the tank. Information is needed on the temperature lag relative to the conditions inside the tank. Fortunately a phenomenon occurred during blowdown Run No. 2 (Fig. 9) which permits a determination to be made of the temperature lag of the thermocouple element. If the curves of Fig. 9 are examined, it will be found that a hump occurs in curves 1, 2, and 3 when the temperature 480°R is reached. These humps are almost certainly caused by the freezing of supercooled water on the element. As will presently be seen, this amount of water is quite small and is probably distributed as small droplets on the surface of the element. The important point, however, is that the freezing of the supercooled water provides something approximating a discontinuous temperature change and establishes a new slope to the cooling curve of the thermocouple. If the slope were known exactly, the temperature lag could be determined exactly, but the curves are of necessity faired to the points with a certain degree of inaccuracy and therefore the slopes are known only approximately. Nevertheless, the curves provide a valuable approximation to the temperature lag and are used for this purpose.

Consider the basic equation for heat transfer across a boundary

$$q = hA\Delta T,$$

where

q = heat flux, Btu/hr

h = heat transfer coeff, Btu/(hr)(ft^2)(°F)

ΔT = Temperature difference across the boundary, °F

A = area of boundary, ft^2

Also consider an idealized cooling curve of the type obtained in Run No. 2 (Fig. 42).

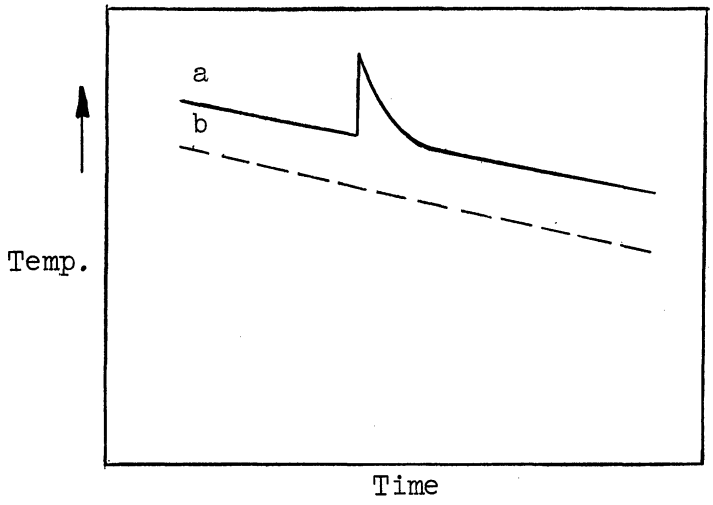

Fig. 42 (a) Idealized curve of thermocouple temperature and (b) true air temperature during tank blow-down run.

Let curve a represent the temperature of the thermocouple and curve b the true temperature of the air. At any point on curve a the value of q may be ascertained, and it is proportional to the slope of the curve at that point. The area A in the basic equation is known from the dimensions of the thermocouple.

The values of q and A_2 are now known for the basic equation. To obtain a solution, two independent values involving q and Δt will be required, since Δt is not known directly but is known at any two points relative to the unknown true air temperature. Returning to the curves of Fig. 9, the following observations are made:

Average temperature at start of humps, 480°R
Average temperature at top of humps, 483.7°R
Average heat flux immediately ahead of humps, 33.4 Btu/hr
Average heat flux on cooling slope of humps, 93.7 Btu/hr
Melting temperature of ice, 492.0°R

The mass of the thermocouple element (0.1 in, in diameter) is calculated as 1.6×10^{-4} lbs. Surface area of the thermocouple is 2.18×10^{-4} ft^2. The specific heat of the thermocouple is 0.08. Substituting into the basic equation,

$$(33.4)\ (.08)\ (1.6 \times 10^{-4}) = h\ (2.18 \times 10^{-4})\ (480 - T_{air})$$
$$(93.7)\ (.08)\ (1.6 \times 10^{-4}) = h\ (2.18 \times 10^{-4})\ (485.7 - T_{air})$$

The solution gives

$$h = 0.6206 \text{ Btu/(hr)}(ft^2)(°F)$$
$$T_{air} = 476.84°R$$
$$\Delta T = 3.16°F \text{ or } °R$$

ΔT measured at the start of the hump then represents the temperature lag between the air and the thermocouple. According to the preceding method of evaluation, the temperature error, ΔT, may then be taken as proportional to the rate of change of temperature as measured by the thermocouple. The temperature correction is

$$\Delta T = 340°F \frac{dT}{dt}$$

where dT/dt = rate of temperature change of element, °F/sec. The value of h so determined (0.6206) agrees in order of magnitude with the value calculated for cylinders of the same diameter as the thermocouple, from McAdams simplified equation;*

$$h = 0.27\ (\Delta t/D)^{0.25}$$
$$h = 1.18 \text{ Btu/(hr)}(ft^2)(°F)$$

It is of interest to calculate the amount of moisture which adheres to the thermocouple at the time of freezing. It will be recalled that supercooled water releases the heat of fusion on freezing, so that for a thermally isolated sample the result of freezing is an equilibrium mixture of water and ice existing at 32°F. It is this heating effect of the freezing process that raises the temperature of the thermocouple. In this case, the mass of the thermocouple is so large relative to the mass of the supercooled water that all the water freezes before the thermocouple is heated to 32°F. It is necessary, then, to formulate a heat balance which equates the heat gained by the thermocouple to that given up by the supercooled water in the process of freezing and adjusting to the final temperature.

*McAdams Wm. H., Heat Transmission, page 241.

Let T_1 = average thermocouple temperature at start of hump, °R

T_2 = average thermocouple temperature at top of hump, °R

T_3 = melting point of ice, °R

M = mass of thermocouple element, lbs

m = mass of supercooled water on thermocouple element, lbs

L = latent heat of fusion of ice, Btu/lb

C_i = specific heat of ice, Btu/lb

C_e = specific heat of the thermocouple elements, Btu/lb

The heat balance is then written:

$$(T_2 - T_1)\, Mc_e = L\, m \left(1 - \frac{T_3 - T_1}{L}\right) + (T_3 - T_2)\, m\, C_i.$$

Substituting the known quantities gives

$$(3.7)(1.6 \times 10^{-4})(0.08) = 144 \left(1 - \frac{12}{144}\right)m + (8.3)(0.5)m \text{ and } m = 3.47 \times 10^{-7} \text{ lb.}$$

It is evident that the amount of water attached to the thermocouple is quite small and has a notable influence only because of the large heat of fusion of water.

It should be remarked here that the water attached to the thermocouple must have been deposited there by the impingement of condensed water droplets suspended in the air at the start of the run. Thermodynamic considerations make any other mechanism improbable. It should also be noted that the freezing of supercooled water on the elements has been observed on only one run. Evidently, some particular conditions are necessary for the phenomenon to develop. The most likely condition seems to be that the elements have condensed moisture on them before the start of the run. The phenomenon may have some general application and it would be interesting to study it further.

APPENDIX B

ORIFICE METER CALIBRATION

Three different square-edge orifices were used to measure the air flow. These orifices were 1, 2, and 4 inches in diameter. They were placed in a 6-inch steel pipe which was provided with radius pressure taps.

The flow calibration of the orifices was undertaken as follows: A calibration run was started with the air tank filled nearly to capacity. The air flow rate was adjusted until a predetermined differential pressure was obtained across the orifice. Meanwhile, the air temperature and pressure in the tank were recorded as a function of time. The air stagnation temperature at the orifice was also measured. During the run the orifice differential pressure would be changed to a second predetermined value without interrupting the flow.

By using the data thus taken, the mass of air in the tank was calculated and plotted as a function of time. The slope of this curve gave the mass air discharge rate from the tank at any time. This mass discharge rate was used with the orifice reading to calibrate each orifice. By changing the orifice ΔP during the run, two discrete slopes in the mass discharge curve were obtained. This technique increased the number of calibration points. The difficulties of manual adjustment and data recording made producing more than two discrete slopes in the mass discharge curve unreliable.

The form of the equation used for the flow calibrations is as follows:

$$w = KY \sqrt{\frac{\Delta P \cdot P}{T}} ,$$

where

w = air mass flow rate, lbs/sec

K = orifice coefficient (includes the area term)

Y = expansion factor

ΔP = static pressure differential across orifice, inches Hg,

P = upstream static pressure, inches Hg,

T = stagnation air temperature, °R.

When used in this manner, the orifice coefficient contains the area term for a particular orifice and also the necessary conversion terms for the use of pressure in inches of mercury.

The expansion factor Y depends primarily on (1) the specific heat ratio of the fluid, (2) the diameter ratio of the orifice to the pipe, and (3) the pressure ratio across the orifice. In this instance, only the pressure ratio varies significantly with a given orifice. The value of Y may be calculated, but it is more conveniently read from a plot which takes the above factors into consideration*.

An interesting feature of the air system used is that, regardless of the temperature of the air in the storage tanks, the temperature of the air as it reaches the orifice meter is practically constant, varying only a few degrees from 495°R. This situation is not readily explained, but must be related to the heat transfer into the long pipe that delivers air to the test site. Apparently, the effective heat transfer into the pipe increases greatly when frost begins to form on the pipe since both the heat of condensation and the heat of freezing of the water vapor are effective in releasing heat. If the run were continued for a long enough time the frost coating itself would become thick enough to provide an effective barrier to heat transfer, but in the practical case, the air supply is exhausted before this happens. This behavior of the air supply system makes it practically unnecessary to include the temperature as a seperate item in the orifice formula, which then becomes:

$$w = KY \sqrt{P\Delta P}$$

The temperature term becomes a part of the constant K. For those conditions where the orifice temperature varies considerably from 495°R, K should be modified by the relation

$$K_1 = K \sqrt{T/T_1}$$

The orifice flows are therefore expressed as follows:

For 1-inch orifice, $w = .0130\ Y \sqrt{P\Delta P}$
2-inch orifice, $w = .0481\ Y \sqrt{P\Delta P}$
4-inch orifice, $w = .272\ Y \sqrt{P\Delta P}$

The quantities expressed above for the orifice coefficient are averages calculated from several runs. Individual runs gave results that varied as much as 10 per cent from these average values. The source of this error has not been ascertained; it is very puzzling because orifice meters are ordinarily supposed to give results accurate to within 2 per cent without

* "Fluid Meters - Their Theory and Application" Part I, 4th Ed. A.S.M.E.

the need for extraordinary precautions. The most convenient way to explain the error is in the measurement of pressures and temperatures in the tank, but these measurements could at most contribute an error of about 5 per cent to the calculated flow constant. The major source of error is probably the large pressure differentials at which the orifices were used.

Some previous work was done using the orifices at small pressure differentials relative to the absolute pressure. Under these conditions, it was not as difficult to get reliable performance from the orifices. It appears that this is the most satisfactory way to use an orifice flowmeter.

In order to secure an independent check on the orifice coefficient, a series of tests was made to calibrate the orifice against sonic nozzles. Three nozzles of circular entrance section were made, the nozzle diameters being 0.5 inch, 1.0 inch, and 1.5 inches, respectively. These nozzles were placed downstream of the orifice plate and the runs were made so that supercritical pressures were obtained at the nozzles. The corresponding orifice pressures and temperatures were measured. Using this method, the flow coefficient for the orifices were calculated as follows:

For 1-inch orifice $w = 0.0191 \sqrt{P\Delta P}$,
2-inch orifice $w = 0.0402 \sqrt{P\Delta P}$,

The expansion factor is included in the constants, which would have to be modified if the pressure ratio were changed, but the data appear useless as a check, because the constant used in this flow formula should be about 4 times as large for a 2-inch orifice as for a 1-inch orifice, while the ratio of the constants here is only 2 to 1. The constants obtained from the tank pressure-temperature runs follow the ratio rule fairly well, and therefore, these data are probably more reliable and were used in the report. Altogether, the flow measurements obtained from the orifice meters have been a source of considerable difficulty and are considered to be unsatisfactory. It is apparent that a more reliable method of flow measurement is needed.

APPENDIX C

PROJECTED OPENING OF A BUTTERFLY VALVE

In the earlier report on butterfly valves, no correction was made for the effect of plate thickness on the projected valve opening, and for this reason, the flow coefficients are based on a projected opening that is larger than the actual projected opening. No correction for plate thickness has been made in this report either, but it is of interest to examine the matter in order to determine the magnitude of the error. As stated before, the equation for the projected opening of a thin-plate valve is $A_\beta = A_o (1 - \cos \beta)$,

where

A_β = projected opening along the flow axis

A_o = area of the duct with the valve plate removed

β = angle of opening measured from the closed position.

Assume that the valve plate surfaces are spherical. The following diagram (Fig. 43) is a cross section of the valve plate where it is assumed that the axis of the valve shaft is normal to the paper.

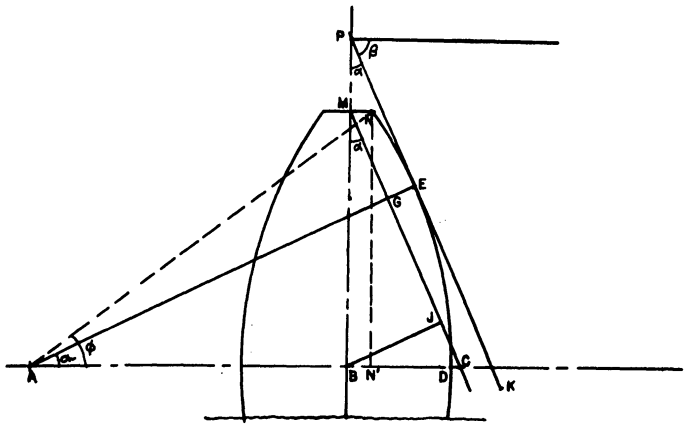

Fig. 43 Geometry of the Projected Opening of the Valve
β from 90° - ϕ to 90°

Take the axis of the duct to be along the line PK. This means that the valve is set at angle β from the closed position, according to convention. The projected opening of the thin plate is proportional to BJ and that added by the spherical surface is proportional to GE. The projected opening is then proportional to MB-(BJ + GE) and this holds until $\sigma = \phi$. Geometric considerations show that

$$\sigma = \alpha = 90°-\beta$$

$$BJ = MB \sin \alpha$$

$$BC = MB \tan \alpha$$

$$AC = r-BD + BC = r-BD + MB \tan \alpha$$

$$AG = AC \cos \alpha = (r-BD + MB \tan \alpha) \cos \alpha$$

$$GE = r-AG = r - (r-BD + MB \tan \alpha) \cos \alpha .$$

The projected opening is then proportional to

$$MB- [MB \sin \alpha + r - (r-BD + MB \tan \alpha) \cos \alpha] .$$

The fractional opening is $\frac{(MB-r) + (r-BD) \sin \beta}{MB}$. The projected opening is therefore

$$A_\beta = A_o \frac{(MB-r) + (r-BD) \sin \beta}{MB} .$$

This relation holds from $\beta = 90°-\phi$ to $\beta = 90°$ and $\phi = \sin^{-1} BM/r$.

The relationship which holds from $\beta = 0$ to $\beta = 90°-\phi$ should now be examined, (See Fig. 44) The projected opening is proportional to BM-BE and to BE-BP sin α.

$$BP = BM + MP$$

$$MP = \frac{MN}{\tan \alpha}$$

$$BP = BM + \frac{MN}{\tan \alpha}$$

$$BE = (BM + \frac{MN}{\tan \alpha}) \sin \alpha$$

$$BE = BM \sin \alpha + Mn \cos \alpha .$$

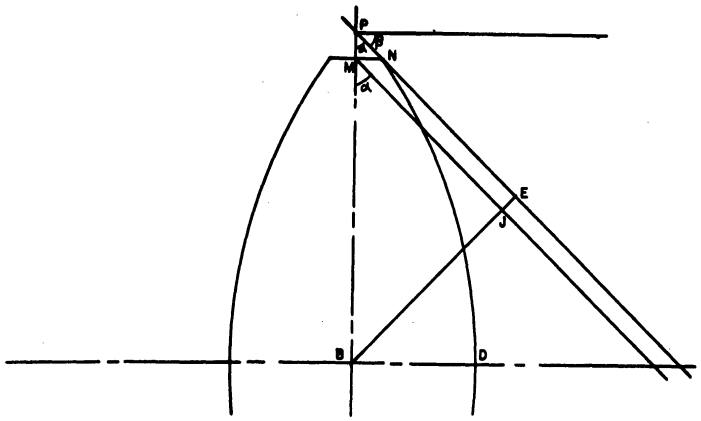

Fig. 44 Geometry of the Projected Opening of the Valve
β from 0° to 90°-φ

The projected opening is therefore:

$$A_\beta = A_o \frac{BM - BM \cos\beta - MN \sin\beta}{BM} = A_o \frac{BM\,(1-\cos\beta) - MN \sin\beta}{BM}$$

This relation holds from $\beta = 0°$ to $\beta = 90°-\phi$.

It should be noted that the relations developed above hold only for plates where all the cross sections are circular arcs and where the radius is proportional to the chord. The exact solutions for the spherical shape where all cross sections are not similar would be considerably involved, but the above relation is a good approximation where the plate surfaces subtend less than one radian, based on the spherical radius.

In the following graph (Fig. 45) the valve openings are compared for a thin plate and for the actual plates used in the 6-inch circular valve.

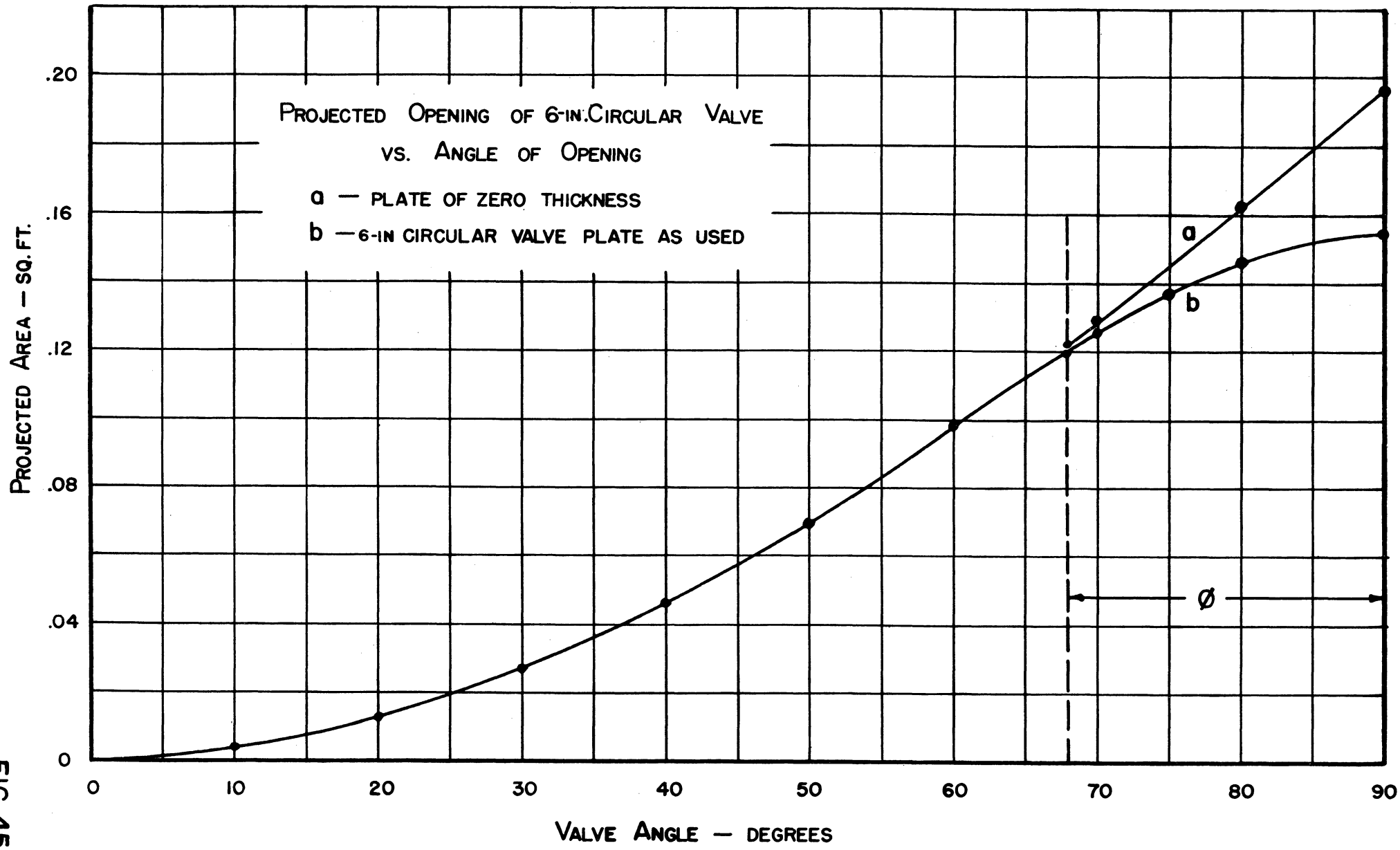
PROJECTED OPENING OF 6-IN. CIRCULAR VALVE
VS. ANGLE OF OPENING
a — PLATE OF ZERO THICKNESS
b — 6-IN CIRCULAR VALVE PLATE AS USED
PROJECTED AREA — SQ. FT.
.20
.16
.12
.08
.04
0
0
10
20
30
40
50
60
70
80
90
VALVE ANGLE — DEGREES
a
b
Ø

FIG. 45